5-3-2019

# Investigations on Stabilized Sensitivity Analysis of Chaotic Systems

Lamiae Taoudi

# Investigations on stabilized sensitivity analysis of chaotic systems

By

Lamiae Taoudi

A Thesis
Submitted to the Faculty of
Mississippi State University
in Partial Fulfillment of the Requirements
for the Degree of Master of Science
in Computational Engineering
in the Department of Computational Engineering

Mississippi State, Mississippi

May 2019

Investigations on stabilized sensitivity analysis of chaotic systems

By

Lamiae Taoudi

Approved:

---

Manav Bhatia
(Major Professor /Graduate Coordinator)

---

Shantia Yarahmadian
(Committee Member)

---

J. Edward Swan II
(Committee Member)

---

Jason M. Keith
Dean
Bagley College of Engineering

Name: Lamiae Taoudi

Date of Degree: May 3, 2019

Institution: Mississippi State University

Major Field: Computational Engineering

Major Professor: Dr. Manav Bhatia

Title of Study: Investigations on stabilized sensitivity analysis of chaotic systems

Pages of Study: 86

Candidate for Degree of Master of Science

Many important engineering phenomena such as turbulent flow, fluid-structure interactions, and climate diagnostics are chaotic and sensitivity analysis of such systems is a challenging problem. Computational methods have been proposed to accurately and efficiently estimate the sensitivity analysis of these systems which is of great scientific and engineering interest. In this thesis, a new approach is applied to compute the direct and adjoint sensitivities of time-averaged quantities defined from the chaotic response of the Lorenz system and the double pendulum system. A stabilized time-integrator with adaptive time-step control is used to maintain stability of the sensitivity calculations. A study of convergence of a quantity of interest and its square is presented. Results show that the approach computes accurate sensitivity values with a computational cost that is multiple orders-of-magnitude lower than competing approaches based on least-squares-shadowing approach.

Key words: Chaos, Bifurcation study, Direct sensitivity analysis, Adjoint sensitivity analysis

ACKNOWLEDGEMENTS

I would like to seize this opportunity to thank my advisor, Dr. Manav Bhatia, for his guidance, his patience and his support for me during my research work. My thanks are also extended to all of the committee members, Dr. Shantia Yarahmadian and Dr. John E. Swan, for their advices and their valuable involvement to improve my work.

I would also like to thank my friends in Starkville, for their constant support throughout this process and for making these years an unforgettable experience.

Lastly and most importantly, I would like to express my profound gratitude to my parents Lalla Zineb Lamraoui and Abdelmajid Taoudi, and my sister Fatima Zohra Taoudi for their unconditional love, and a heartfelt gratefulness for my brother Amine Taoudi for his untiring moral support and encouragement throughout this project period. I would therefore like to dedicate this thesis to my entire familly.

TABLE OF CONTENTS

LIST OF FIGURES

# CHAPTER I

# INTRODUCTION

Chaos is derived from a Greek word originally used to define the infinite empty space before everything existed [1]. In recent years, the word chaos means a state of disorder and irregularity. In the field of mathematics, Chaos is defined as an aperiodic long term behavior in a deterministic system that exhibits sensitive dependence on initial conditions [2]. This means that the trajectories of a system that does not have random or noisy inputs and parameters, do not settle down to fixed points, periodic orbits or quasiperiodic orbits. However, the nearby trajectories separate exponentially fast. Chaotic behavior can be seen in different nonlinear systems describing physical or environmental phenomena such as weather forecasts [3], turbulent flow[4], population modeling [5], economics [6], etc.

Nonlinear systems exhibiting chaos became of great interest starting from 1963, owing to a meteorologist named Edward Lorenz who derived a set of three quadratic ordinary differential equations as a simplified model of atmospheric convection[3]. Lorenz discovered thanks to his computer modeling that his system could display a very complex behavior. His system's response was highly unpredictable, such that a slight difference in one of the system's variables had a drastic effect on the whole system's response. This is referred to as sensitive dependence on initial conditions. Lorenz also gave a graphic representation of

the solution of his equations using his computer. Plotting his solution on an xz plane, he found an attractor that had a shape of a butterfly. His findings gave rise to the term of the "Butterfly Effect".

In order to understand this phenomena, Ruelle, a Belgian physicist, studied attractors and called Lorenz attractor as a strange attractor since the trajectories in the phase space seem to form cycles but don't intersect with each other [4]. Because they are not on the same plan and not concentric. Bifurcation studies were used to quantitavely monitor the topological changes of a system's solution as a parameter is varied. These studies help understand the nonlinear systems without having to solve them numerically. Many bifurcations can be seen in nonlinear dynamical systems, such as saddle node bifurcations, hopf bifurcations, limit cycle oscillations, period doubling, flip or fold bifurcations, etc [7].

In recent years, applied mathematicians and engineers are becoming more interested in studying these nonlinear dynamical systems and quantifying the sensitivity of the systems' responses with respect to their parameters. Sensititivity analysis is widely used in a large range of physical and engineering problems such as: aerodynamic shape optimization [8], adaptive grid refinement [9], and data adjustment for weather forecasting [10]. Sensitivity analysis can be computed either with a direct method or an adjoint approach. The forward or direct method is more efficient for computing sensitivity derivatives of many output quantities to a few input parameters, whereas the adjoint method is more efficient for computing sensitivity derivatives of a few output quantities to many input parameters.

In the past few years, sensitivity analysis of chaotic systems became important for design optimization. Time instantaneous quantities of these systems cannot be used as a

design metric because of their random nature and their lack of convergence, therefore time-averaged quantities are used as quantities of interest. Since the computational capacity of computer improved, many methods have been proposed to accurately compute the sensitivity values of these nonlinear systems. Methods, such as ensemble averaging method [11], least-squares-shadowing (LSS)[12], non-intruisive LSS method [13] has been proposed but are computationally expensive.

In this thesis a new approach of computing the sensitivity analysis of chaotic systems is presented. This method, developed by Bhatia and Makhija [14], is able to compute accurate direct and adjoint sentivity values of time-averaged quantities by using a stablized sensitivity solver [15]. Adaptive time-step control is used to maintain stability of the sensitivity calculations of two nonlinear systems: the Lorenz system and double pendulum.

This thesis is organized as follow: the following chapter presents a literature review of chaos theory and sensitivity analysis. Chapter 3 focuses on chaos in Lorenz system and its bifurcation study. Chapter 4 introduces sensitivity analysis of chaotic systems and discusses the current approach. Results of the sensitivity analysis of the Lorenz system are given in Chapter 5. Chapter 6 presents the double pendulum system, its chaotic behavior and its sensitivity analysis. Finally, Chapter 7 gives a summary of this thesis along with some conclusions and future research directions.

# CHAPTER II

# LITERATURE REVIEW

## 2.1 Previous work in chaos theory

Chaos theory is a branch of mathematical theory that is still in development. It describes a series of phenomena rising from nonlinear dynamical systems. These systems are mathemtical models to natural problems that scientists try to understand and interpret using mathematical equations.

In the seventeenth century, Kepler, Galileo, and Descartes discovered the laws of motion and the causality effect principle, which states that each effect has a cause [16]. Isaac Newton later validated this principle and developed laws of celetial motions independent of the initial conditions. These differential equations show the variation of quantities with respect to time and were called a two-body problem. However, as the number of planets or variables increase the problem becomes complex and requires new analytical methods to solve it.

Years later, the mathematician and astronomer Pierre Simon Laplace worked on the concept of universal determinism. Determinism is another way of expressing the causality effect, such that every event is physically determined by a series of previous causes[17]. Laplace was also able to use Newton's laws of motion to calculate the past and future trajectories of the solar system based on the initial condition of the systems.

In 1885, Henri Poincaré, a french mathematician, tackled the many-body problem that Newton could not solve. In his paper, he analyzed a three-body problem and derived a result that demonstrated the stability of the solar system. He defined the state of the system at a given moment represented in the phase space. Years later, Poincaré found very complex geometries that were related to chaotic behavior of the solar system [18]. He also discovered the phenomenon of sensitivity to initial conditions when he noticed that a slight difference in the initial position of the planets resulted in huge differences in their position in the long run. This was the birth of the chaos theory.

In the 1960s, a meteorologist found similar conclusions. From the Massachusetts Institute of Technology, Edward Lorenz is considered as the official discoverer of chaos theory. This occured while programming 12 weather-simulating equations into his vacuum tube computer to predict weather changes. The equations he used were similar to those Poincaré and Newton had studied before and were proved extremely difficult to solve. Lorenz found that two slightly different initial conditions (0.506 instead of 0.506127) gave rise to extremely different behavior [3]. This conclusion was similar to Poincaré's and was then named sensitive dependence on initial conditions. It was then refered to as the butterfly effect based on the title of Lorenz presentation given by Philip Merilees, the meteorologist who organized the 1972 conference session where Lorenz presented his result, which was "Predictability: does the flap of a butterfly's wing in Brazil set off a tornado in Texas?"[19]. Lorenz not only showed that a perfect weather prediction is impossible but also rediscovered the chaotic behavior of nonlinear dynamical systems. Moreover, Lorenz presented a graphic description of his results using his computer and the figure that appeared was his

second discovery: the attractors. Fig. 3.17 represents the Lorenz attractor in the xz plane for $\rho = 28$, $\beta = 8/3$ and $\sigma = 10$.

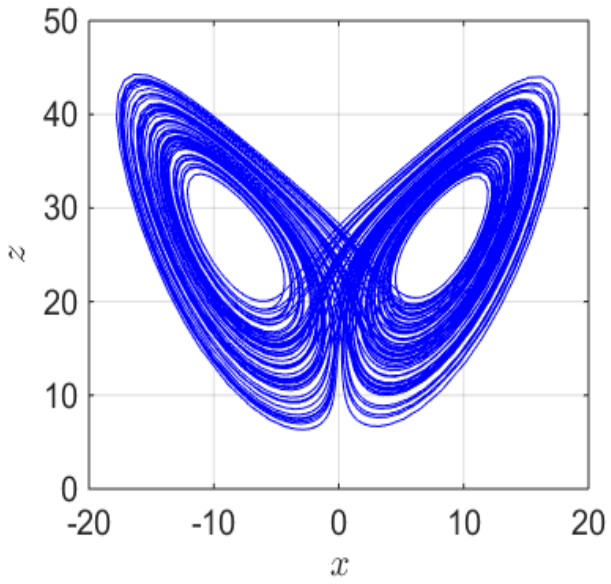


Figure 2.1: Lorenz attractor of Lorenz system.

David Ruelle assigned the term of "strange attractor"[4] to this phenomena. Strange attractors can be a representation of a chaotic system in a specific phase space. However, attractors can also be found in various nonchaotic dynamical systems. There are four types of attractors: fixed point, limit-cycle, limit-torus, and strange attractor. While working on turbulent flows, Ruelle and Takens argued that the Navier-Stokes equations also exhibited strange attractors, and that the onset of turbulence is a result of the presence of these attractors [4].

After Lorenz, more strange attractors were discovered. From a chemical reactions study, the R*ö*ssler attractor was found. Chua attractor came out from the study of an electronic circuit [7].

Period doubling is another behavior that can be observed in chaotic systems. It was proposed by Mitchell Jay Feigenbaum to describe the transition between regular dynamics and chaos in a system while studying the logistic map proposed by the biologist Robert May [20], [21]. This system's behavior changes depending on the value of its variable r. Periodic orbits are observed and period doubling occurs as the value of r (growth rate) increases as seen in Fig. 2.2 versus the long term x the quantity of interest.

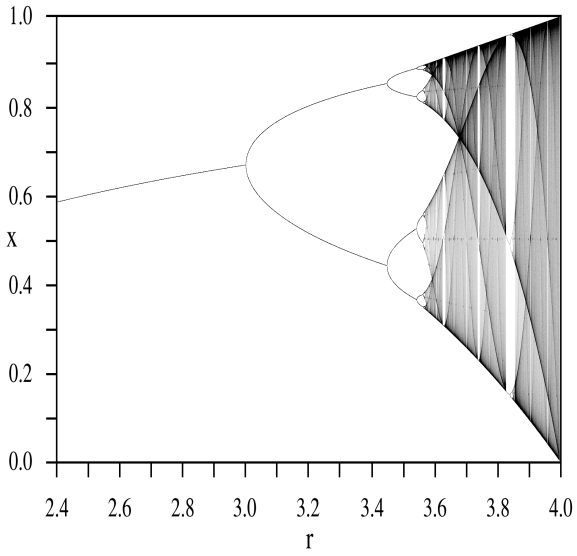


Figure 2.2: Bifurcation diagram of logistic map [16].

Chaos theory is an area of interdisciplinarity. Lorenz, a meteorologist, Ruelle, a mathematical phisict, and other mathematicians, chemists, and biologists were working on sim-

ilar things. The modern chaos theory would not have been possible without computers to perform millions of operations in a short period of time. Nowadays, engineers have become interested in understanding nonlinear chaotic systems and performing design optimization on these systems.

## 2.2 Stability of dynamical systems

The notion of stability is very important in chaos theory. Considering a dynamical system which satisfies

$$\dot{x} = f(x,t) \qquad x(t_0) = x_0 \qquad x \in R^n, \tag{2.1}$$

$f(x,t)$ is Lipschitz continuous with respect to $x$, uniformly in $t$, and piecewise continuous in $t$. If a point $x^* \in R^n$ satisfies $f(x^*,t) = 0$, then $x^*$ is an equilibrium point of Eq. 2.2.

$x^*$ is locally stable if all solutions which start near it remain close to it for all time. The equilibrium point $x^*$ is said to be locally asymptotically stable, if $x^*$ is locally stable and, all solutions starting in a neighborhood of $x^*$ tend towards $x^*$ as $t \to \infty$. $x^*$ is globally stable, if it is stable for all initial conditions $x \in R^n$ [22].

If the origin of the system is shifted, the equilibrium point occurs at $x^* = 0$.

### 2.2.1 Definition of asymptotic stability

The equilibrium point $x^* = 0$ is asymptotically stable at $t = t_0$ if, $x^* = 0$ is stable and $x^* = 0$ is locally attractive. Uniform asymptotic stability requires $x^* = 0$ to be uniformaly stable, and $x^* = 0$ is uniformally locally attractive. $x^* = 0$ is unstable, if it is not stable [22].

### 2.2.2 Definition of Lyapunov stability

The equilibrium point $x^* = 0$ is stable at $t = t_0$ if for any $\epsilon \geq 0$, there exists a $\delta(t_0, \epsilon) \geq 0$ such that

$$||x(t_0)|| \leq \delta \quad \rightarrow \quad ||x(t)|| \leq \epsilon, \quad \forall t \leq t_0. \tag{2.2}$$

If $\delta$ is not a function of $t_0$, Uniform stability is guaranteed and the origin will not lose stability.

Lyapunov stability is a weak requirement on equilibrium points. It is defined only at a time instant $t_0$. It also does not require that the trajectories starting near the equilibrium point tend to it asymptotically [22].

### 2.2.3 Definition of exponential stability

The equilibrium point $x^* = 0$ is exponenatially stable if there exist constants $m, \alpha \geq 0$ and $\epsilon \geq 0$, such that

$$||x(t)|| \leq me^{-\alpha(t-t_0)}||x(t_0)||, \quad \forall ||x(t)|| \leq \epsilon and t \geq t_0. \tag{2.3}$$

The rate of convergence is the maximum value of $\alpha$.

Exponential stability is a stronger stability form. It implies uniform and asymptotic stability. Global exponential stablity can be reached if Eq. 2.2.3 hold $\forall x_0 \in R^n$ [22].

## 2.3 Previous work in sensitivity analysis

Sensitivity analysis determines the mathematical techniques that, when applied to a given system, provide the gradient of an output quantity of interest with respect to design

variables parametrizing the system at hand. It is useful in a large range of physical and engineering problems such as: aerodynamic shape optimization [8], adaptive grid refinement [9], and data adjustment for weather forecasting [10].

The forward or direct algorithms and the adjoint algorithms can be used to compute the sensitvity derivatives. The forward approach is more efficient for computing sensitivity derivatives of many output quantities to a few input parameters, whereas the adjoint method is more efficient for computing sensitivity derivatives of a few output quantities to many input parameters.

In simulations of time-dependent problems mainly chaotic dynamical systems, such as turbulent flows and the climate system, the instantaneous quantities can not be used as a design metric. This is due to their fluctuating nature and their lack of convergence. Therefore time-averaged quantities, such as time-averaged aerodynamic forces in turbulent flow simulations, and the time-averaged global temperature in climate simulations, are of great scientific and engineering interest and computing their sensitivities can be beneficial in many applications.

Traditional sensitivity analyses techniques, both direct and adjoint methods, are used to calculate the sensitivity of the time-averaged quantities with respect to the parameters of the system. The results are obtained by calculating the time-average of the sensitivity, which is done by time averaging the solution of a linear initial value problem obtained from linearization of the dynamics around the reference trajectory [23].

In the field of design optimization with large-scale simulations, adjoint sensitivity approach has been a successful tool [8], [24]. The least-squares-shadowing method is consid-

ered to be state-of-the-art, but is still computationally restrictive even for two-dimensional flows about airfoils [25].

One of the first methods used to tackle sensitivity analysis of time-averaged quantities of chaotic systems was ensemble averaging method [11]. This method yielded good results when direct sensitivity approach was used to study macroscopic climate sensitivity. Eyink et al. went on to generalize the method to solve for sensitivity of ocean circulation and Lorenz 63 [26]. The ensemble adjoint method involves averaging over a large number of ensemble calculations. However, this approach has high computational costs make it uncontrollable for many applications.

The method of least-squares-shadowing (LSS) [12] calculates the sensitivity of chaotic systems using a shadow path of the nonlinear solution, which transforms the problem at hand into a boundary value problem. Even though this method has shown its effectiveness for different low dimensional chaotic systems, it creates a computational challenge for high dimensional systems.

A non-intruisive LSS method has been proposed by Ni et al. [13] as an attempt to reduce the computational cost and the memory usage of the LSS approach. In this method, the sensitivity of long-time-averaged quantities in chaotic dynamical systems has been computed using a tangent solution, which approximates the adjoint and direct sensitivity variables as a linear combination of stable and unstable contributions.

These contributions are detected by computing multiple adjoint and direct sensitivity variables in partitioned segments in time. However, long time segments cause numerical overflow and short segments do not efficiently separate stable from unstable contributions.

This approach has been used to calculate sensitivity analysis of the Lorenz system [12], to resolve turbulent flow about an airfoil [25]. Multiple shooting shadowing for sensitivity analysis of chaotic dynamical systems has been used to solve for chaotic aeroelastic response [27]. Blonigan, et al estimated the cost of approach to be at least four orders-of-magnitude higher than a forward nonlinear solution. Post-processing of several solutions yields the computed adjoint/direct sensitivity variables. Both the number of solutions over each segment and the length of each time segment are tunable parameters. Long time segments produce numerical overflow. Short segments are not able to effectively separate stable from unstable contributions.

The method developed by Lasagna [28] transforms the initial value problem to a boundary value problem using a time-periodic orbit. Both time-averaged quantities and their direct and adjoint sensitivities are calculated on this orbit.

In this thesis, a new approach developed by Bhatia and Makhija [14] is used to calculate sensitivity values and understand their rate of convergence. The solution of the nonlinear dynamical systems is obtained from a nonlinear ODE solver. Nonlinear chaotic dynamical systems can exhibit different responses such as, limit cycle oscillations, period doubling, chaos, etc, but the solution stays contained in a bounded manifold unless an instability forces unbounded growth of the response. The sensitivity equations are a linearization of the chaotic ODE about the nonlinear states. When solving for these sensitivities using conventional approaches on the linearization of chaotic systems, the sensitivity solution grows exponentially, causing round-off errors and numeric overflow. Therefore the linearized sensitivity solution experiences unbounded growth while the nonlinear solution remains

bounded for chaotic systems due to the nonlinearities in the system. The solution of a linear ODE will amplify or decay according to the eigenvalues and eigenvectors of the Jacobian matrix of the linearized ODE, and the applied force function. Stable eigenvalues (real part less than zero) cause decay of the linearized solution and unstable eigenvalues (real part greater than zero) cause growth of the linearized solution. Direct and adjoint sensitivity variables are intermediate quantities whose time-dependent behavior is computed. An inner product with the appropriate function for direct-sensitivity and adjoint-sensitivity yields the sensitivity of the quantity-of-interest with respect to the sensitivity parameter.

# CHAPTER III

## BIFURCATION STUDY OF LORENZ SYSTEM

In 1963, a meteorologist named Lorenz derived a set of three quadratic ordinary differential equations as a simplified model of atmospheric convection from the Navier-Stokes equations. The partial differential equation models the resulting convection motion from a two dimensional fluid cell that is warmed from below and cooled from above. These equations representing three modes, where x, y, and z measure the rate of convective overturning (velocity field), the difference of horizontal temperature, and the distortion of the vertical profile of temperature. These respectively, are:

$$\begin{cases} x' &= \sigma(y-x) \\ y' &= \rho x - y - xz \\ z' &= xy - \beta z \end{cases} \tag{3.1}$$

where the three parameters $\sigma$ (the Prandtl number), $\rho$ (the Rayleigh number), and $\beta$ (an aspect ratio of the region under consideration) are positive. The same equations are used to model lasers, dynamos, chemical reactions, electric circuits, etc [29], [30].

Even though the equations of the Lorenz system seem simple, their solution can be extremely complicated, unpredictable and even chaotic due to the two nonlinear terms: $xz$

and $xy$. For different values of the parameters, the approximate numerical solutions to Eq.(3.1) look complicated. Fig. 3.1 represents the x,z plane projection of the solution for $\sigma = 10$, $\beta = 8/3$,and $\rho = 28$. Looking at the three dimensional picture, the trajectory does not intersect itself. It starts from one side and continues winding from one to the other. It does not settle down to a periodic or stationary behavior.

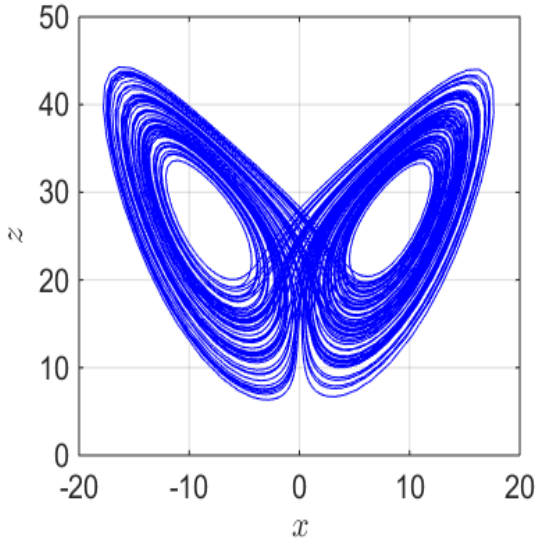


Figure 3.1: A numerical solution to the Lorenz equations projected on the xz plane.

The general form of Fig. 3.1 does not change by varying the initial conditions as long as the initial transient behavior is ignored. However, the trajectory's loops are very sensitive to changes in the initial conditions. This makes the prediction of the trajectory at a certain time interval impossible.

Some of the properties of the Lorenz system are:

- Symmetry: Eq.(3.1) has a symmetry (x,y,z) to (-x,-y,z) for all values of the parameters.

- The z axis: Z axis, x=y=0, is invariant, which means that all trajectories starting on the z axis will remain there and tend towards the origin (0,0,0).

- Existence of a bounded, globally attracting set of zero volume: Lorenz showed that there is a bounded ellipsoid E in $\mathbb{R}^3$ which all the trajectories enter after a certain time. Moreover, the divergence of this system $\frac{\partial \dot{x}}{\partial x} + \frac{\partial \dot{y}}{\partial y} + \frac{\partial \dot{z}}{\partial z} = -(\sigma + \beta + 1)$ is negative. Therefore, there is a bounded set of zero volume within E towards which all the trajectories tend.

- Existence of stationary points: The origin (0,0,0) is a stationary point for all paremeters values. The Lorenz system has two additional stationary points when $1 \leq \rho$.

Chaos has been defined as the high sensitivity to initial conditions, where a small difference in the initial state of a system can cause a big difference in its final state. The first chaotic behavior, observed by Lorenz, was a strange attractor that was called after him as the Lorenz attractor for $\rho = 28$[3]. As the parameters $\sigma, \beta$,and $\rho$ vary, the response's behavior changes in a significant way. Whenever this happens, a bifurcation occurs [31]. Studies have shown that for higher values of $\rho$ the solution becomes chaotic with some periodic windows. In these regions, period doubling bifurcations occur.

### 3.1 Time simulations for different values of $\rho$

Fixing the parameters $\sigma$ and $\beta$ as $\sigma = 10$ and $\beta = 8/3$, $\rho$ is varied as follows:

- Case $\rho \leq 1$:

  In this case, the origin $(x, y, z) = (0, 0, 0)$, shown in Fig. 3.9 and presented as a red star, is the only equilibrium point. All points are attracted to it, including the two initial points used for this simulation $(x_{01}, y_{01}, z_{01}) = (1, 1, 1)$ and $(x_{02}, y_{02}, z_{02}) = (1, -1, 1)$.

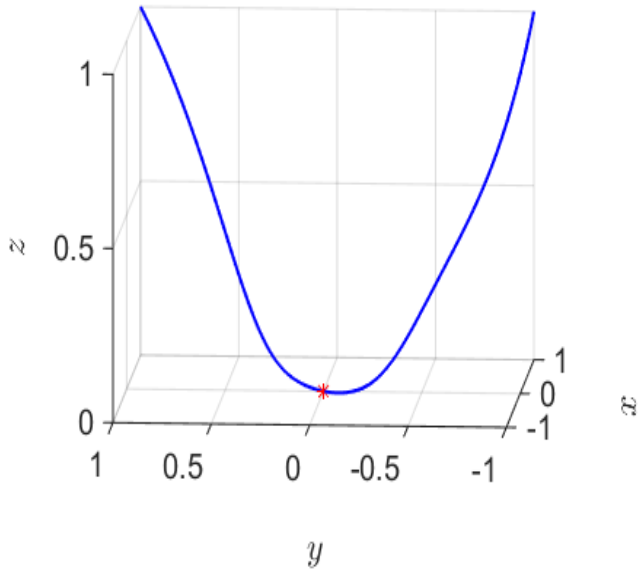


Figure 3.2: Time simulation of the Lorenz system for $\rho = 0.5$.

- Case $\rho = 1$:

  For the case $\rho = 1$, a pitchfork bifurcation is observed where the origin becomes unstable and two stable fixed points appear $(\pm\sqrt{\beta(\rho-1)}, \pm\sqrt{\beta(\rho-1)}, \rho - 1)$.

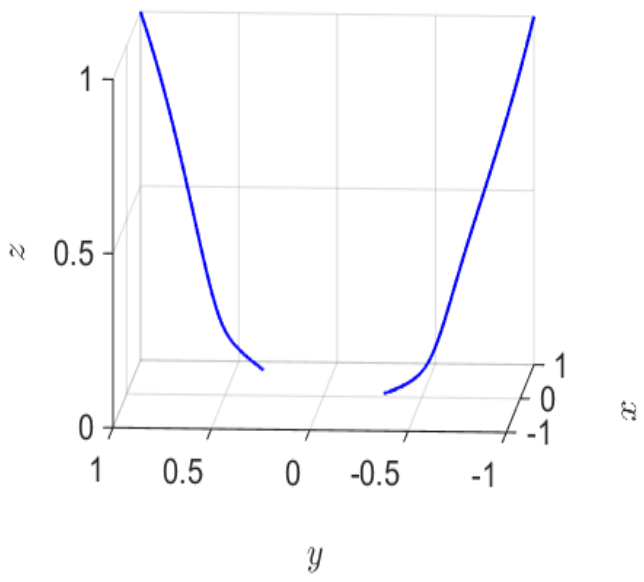


Figure 3.3: Time simulation of the Lorenz system for $\rho = 1$.

- Case $1 \leq \rho \leq 13.925$:

  For the case of $\rho = 10$ shown in Fig. 3.4, two stable manifolds are observed. They are characterized by a trajectory driven away from the origin point $(x, y, z) = (0, 0, 0)$, which for this case is a saddle point, as the time increases. They are starting from their initial points $(x_{01}, y_{01}, z_{01}) = (1, 1, 1)$ and $(x_{02}, y_{02}, z_{02}) = (1, -1, 1)$ and connect to their stable fixed points which correspond to $(x_1, y_1, z_1) = (4.9, 4.9, 9)$ and $(x_2, y_2, z_2) = (-4.9, -4.9, 9)$, respectively.

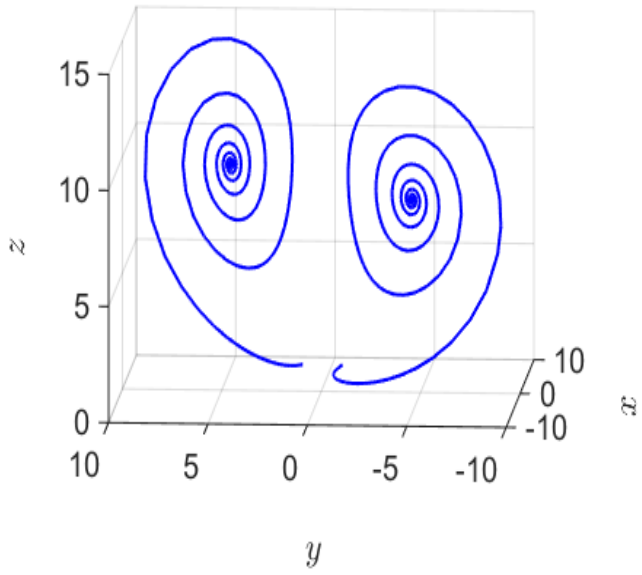


Figure 3.4: Time simulation of the Lorenz system for $\rho = 10$.

- Case $\rho = 13.926$:

  When $\rho = 13.926$, the branches start from the initial points $(x_{01}, y_{01}, z_{01}) = (1, 1, 1)$ and $(x_{02}, y_{02}, z_{02}) = (1, -1, 1)$ and reach the stable fixed points in left and right, respectively. Since the origin $(x, y, z) = (0, 0, 0)$ is unstable, the trajectories cannot pass through it. Therefore, the branches come closer to it without touching it asymptotically which is confirmed in Fig. 3.5. Thus, the stationary orbit at the origin has a homoclinc orbit [31].

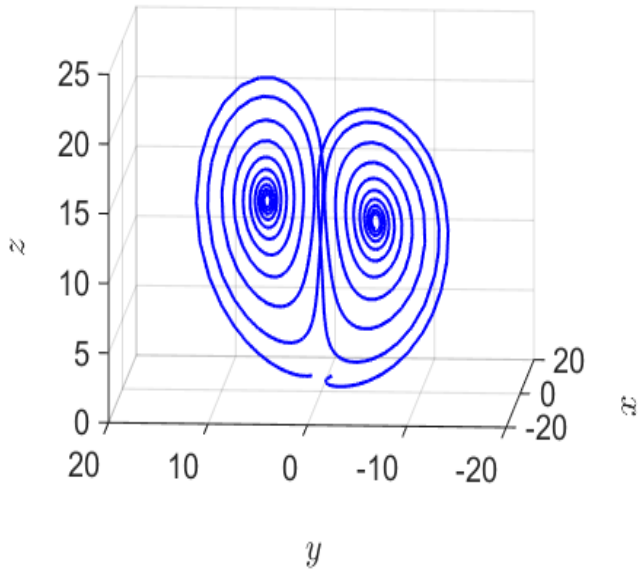


Figure 3.5: Time simulation of the Lorenz system for $\rho = 13.926$.

- Case $13.925 \leq \rho \leq 24.06$:

  For this case where the Rayleigh number $\rho$ equals 20, Fig. 3.6 shows both spirals starting from $(x_{01}, y_{01}, z_{01}) = (1, 1, 1)$ and $(x_{02}, y_{02}, z_{02}) = (1, -1, 1)$, crossing over, and spiraling towards the other side until they reach their corresponding fixed points.

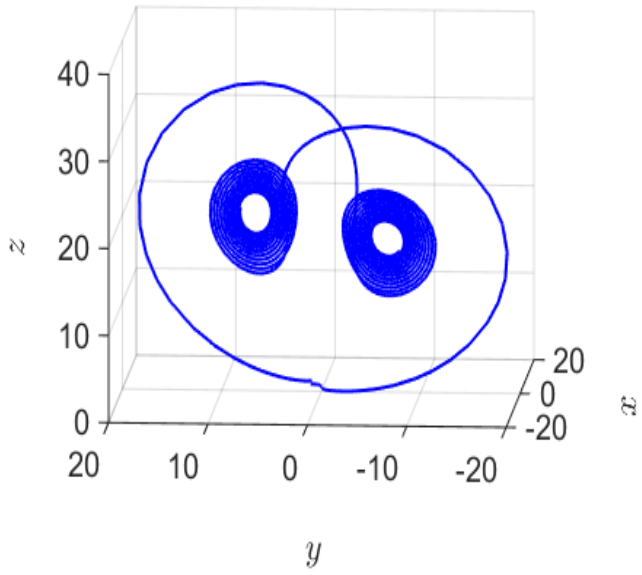


Figure 3.6: Time simulation of the Lorenz system for $\rho = 20$.

- Case $\rho = 24.74$:

  At $\rho = 24.74$, a subcritical Hopf bifurcation occurs. The results in Fig. 3.7 agree with the results shown in the literature. According to Lorenz [3], the two fixed points, observed in Fig. 3.10, Fig. 3.15, Fig. 3.12, lose their stability in the Hopf bifurcation at this value of the Rayleigh number forcing the orbits around them to become unstable.

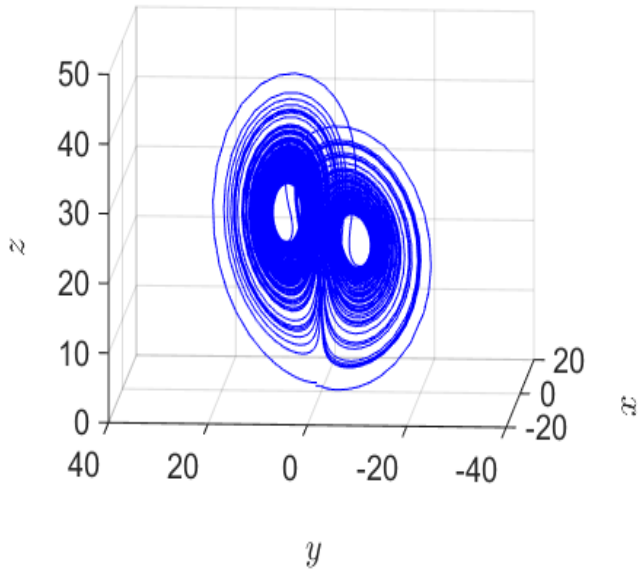


Figure 3.7: Time simulation of the Lorenz system for $\rho = 24.74$.

- Case $\rho = 28$:

  At this value of the Rayleigh number, the Lorenz attractor is observed in Fig. 3.8. Continuation of Codimension 1 bifurcations and limit cycles for this case are presented in the next sections.

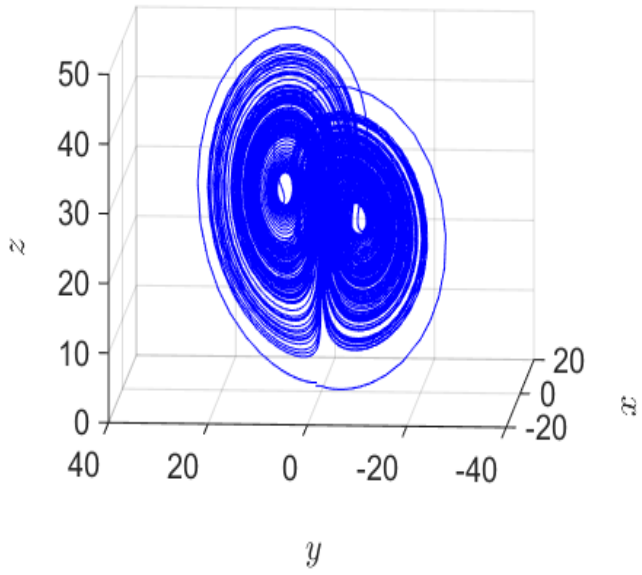


Figure 3.8: Time simulation of the Lorenz system for $\rho = 28$.

- Case $\rho \geq 100.795$:

  Between these two values, period doubling bifurcations of stable periodic points are observed in the time simulations.

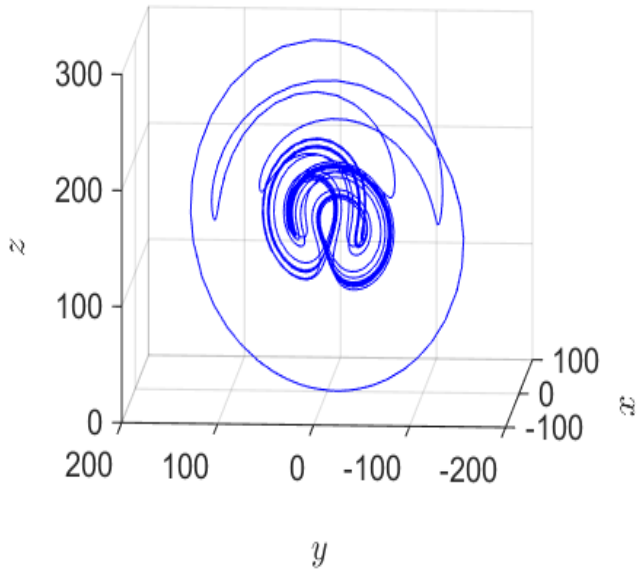


Figure 3.9: Time simulation of the Lorenz system for $\rho = 150$.

## 3.2 Bifurcations study

In this section, a bifurcation study of the Lorenz system is used to qualitatively monitor the behavior of its solution as the control parameters $\sigma$,$\beta$ and $\rho$ are varied. This study uses the Matlab-based bifurcation toolkit, MATCONT, developed by Dhooge, et al [33]. The MATCONT GUI uses the standard Matlab ODE to compute and visualize curves of equilibria, limit points, Hopf points, limit cycles, period doubling bifurcation points of limit cycles, fold, flip and torus bifurcation points of limit cycles.

### 3.2.1 For Rayleigh number $\rho$

a) Continuation of codimension 1 bifurcation of equilibria

To investigate the bifurcations for Rayleigh number $\rho$ for the case of Lorenz attractor

shown in Fig. 3.8, the two other parameters $\sigma = 10$, and $\beta = 8/3$ are kept constant and only $\rho$ is free. Fig. 3.10 shows the bifurcation diagram of the Lorenz system for $\rho = 28$ where the solution exhibits chaotic behavior. For the sake of conformity in all the bifurcation diagrams, the green lines show the stable branches and the red lines show the unstable branch. The blue star (*) shows the location of the Hopf bifurcation, the black star is the Branch Point and the cyan star is the Neutral Saddle. The Hopf points correspond to the value of $\rho = 24.74$ regardless of the initial value of $\rho$.

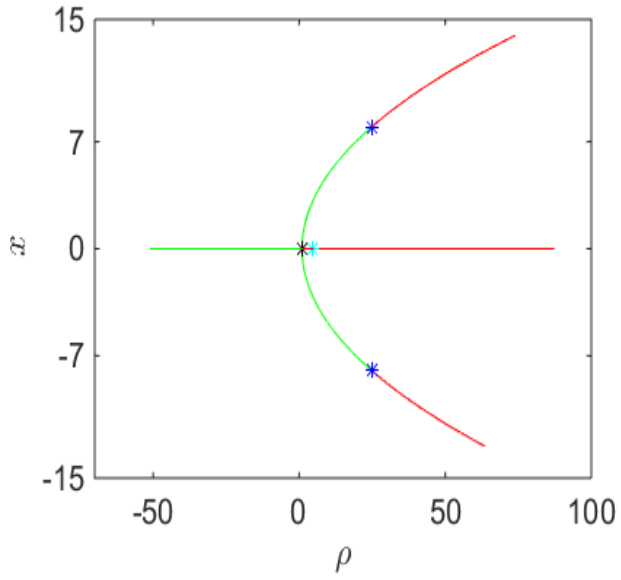


Figure 3.10: Bifurcation diagram of Lorenz system for $\rho$.

b) Continuation of limit cycles

A branch of limit cycles starting from the upper Hopf point is computed. The results

are shown in Fig. 3.11 and no Period doubling bifurcations have been observed for this value of $\rho = 28$.

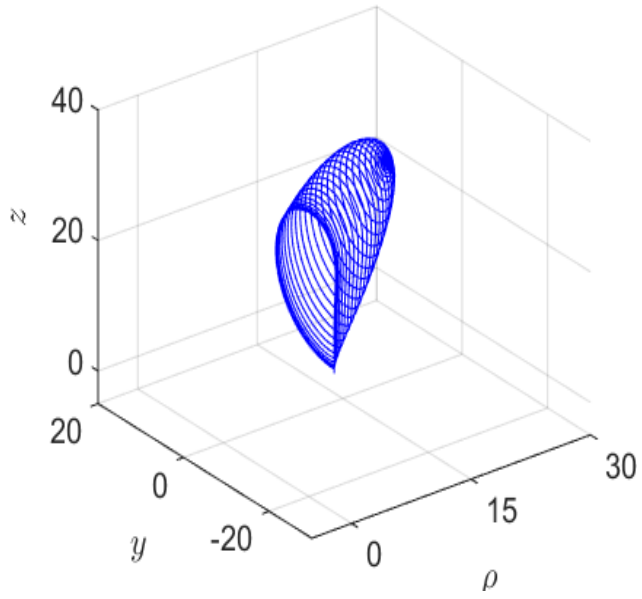


Figure 3.11: Limit cycle continuation of Lorenz system for $\rho$.

### 3.2.2 For Prandtl number $\sigma$

a) Continuation of codimension 1 bifurcation of equilibria

Similar to the previous case, $\sigma$ is set as a free or active parameter while $\rho = 28$ and $\beta = 10$ are kept constant. Fig. 3.12 shows the bifurcation diagram of the Lorenz system for $\sigma$. Two branches have been plotted; the upper one for initial point $(x_0, y_0, z_0) = (1, 1, 1)$ and the lower one corresponds to initial point $(x_0, y_0, z_0) = (0, 0, 0)$. The latter branch is more visible in Fig. 3.12. Two Hopf points and a branch

point are observed in the upper branch. Whereas a Hopf bifurcation, a neutral saddle point, and branch point exist in the lower one. In both branches the stability changes when a Hopf point or a branch point are encountered.

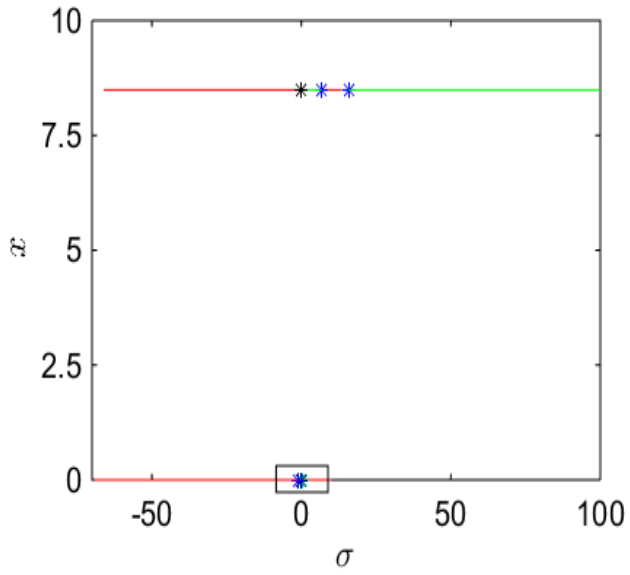


Figure 3.12: Bifurcation diagram of the Lorenz system for $\sigma$.

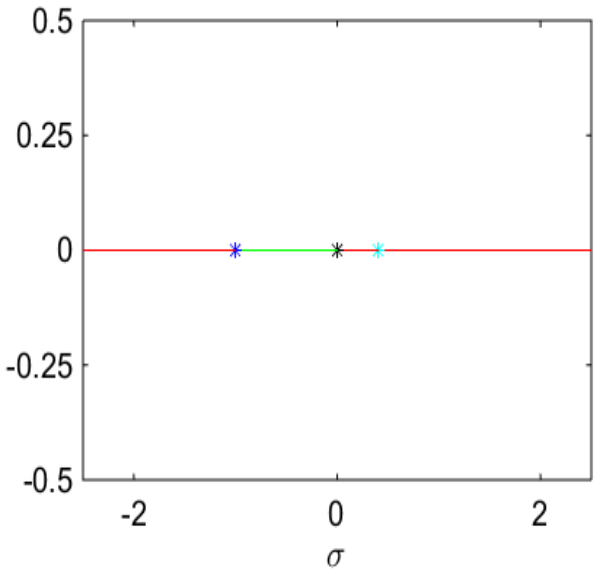


Figure 3.13: Figure 3.12 zoomed

b) Continuation of limit cycles

Starting a limit cycle continuation from a Hopf point of the branch for the initial point $(x_0, y_0, z_0) = (1, 1, 1)$ , the results shown in Fig. 3.14 are generated.

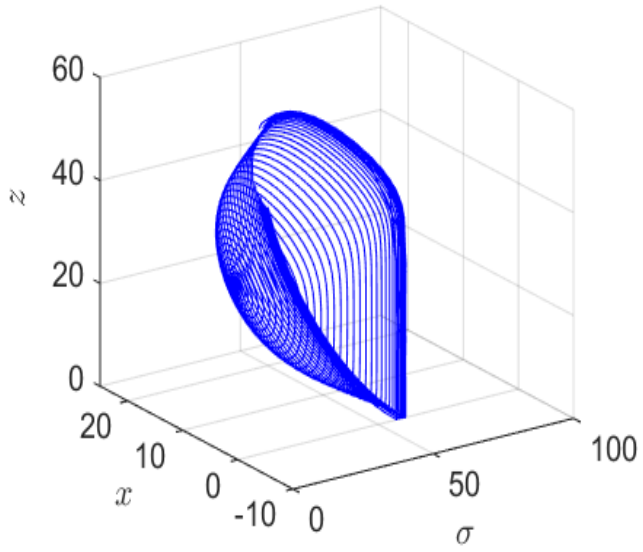


Figure 3.14: Limit cycle continuation of Lorenz system for $\sigma$

### 3.2.3 For the aspect ratio $\beta$

a) Continuation of codimension 1 bifurcation of equilibria

Similar to the previous cases, the investigation of the bifurcations for $\beta$ is started by setting $\beta$ as a free parameter and keeping the other two parameters $\sigma = 10$, and $\rho = 28$ constant. The bifurcation diagram of the Lorenz system for $\beta$ Fig. 3.15 is similar to a supercritical pitchfork bifurcation. This is mainly due to the symmetry property of the Lorenz equations. A branch point, a neutral saddle and two Hopf bifurcations are detected in this case.

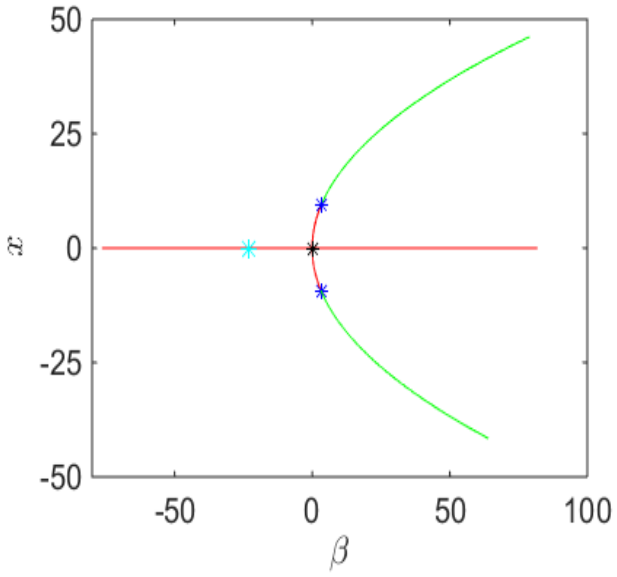


Figure 3.15: Bifurcation diagram of Lorenz system for $\beta$.

b) Continuation of limit cycles and equilibria

The limit cycle continuation from the positive Hopf point is illustrated in Fig. 3.16.

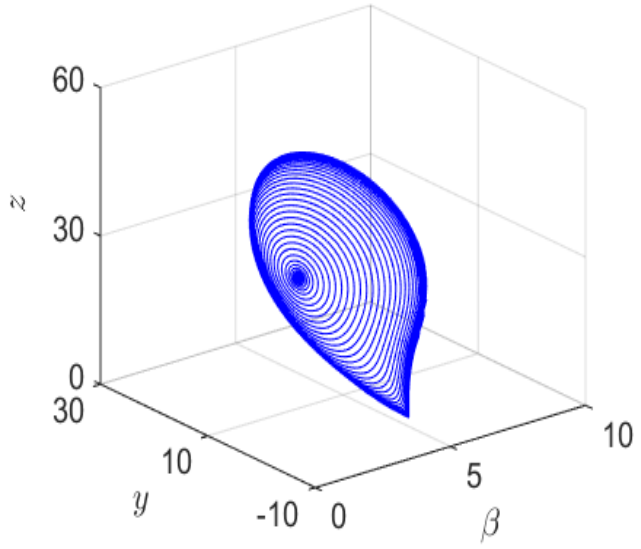


Figure 3.16: Limit cycle continuation of the Lorenz system for $\beta$

### 3.3 Strange attractor

A strange attractor is an attracting set that exhibits high dependence on the initial conditions of the system. Even though the trajectories are very unpredictable, they are attracted to a bounded set. For the Lorenz system they accumulate on the same butterfly shaped object observed in the xz plane projection given in Fig. 3.17 for values of $\rho$ in the range of $24.06 < \rho < 30$.

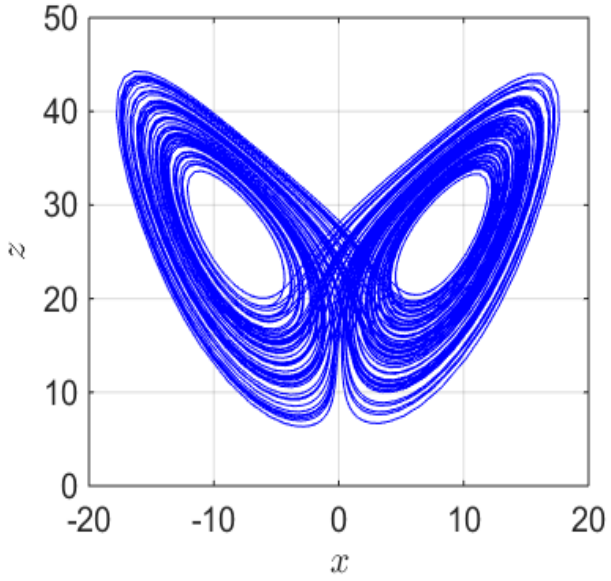


Figure 3.17: Lorenz attractor of the Lorenz system for $\rho = 28$

This accumulation does not seem to depend on the initial position. Considering two close points with a difference of 1.e-3, the two points have the same path at first but their trajectories grow apart as time increases as shown in Fig. 3.18 and then become chaotic.

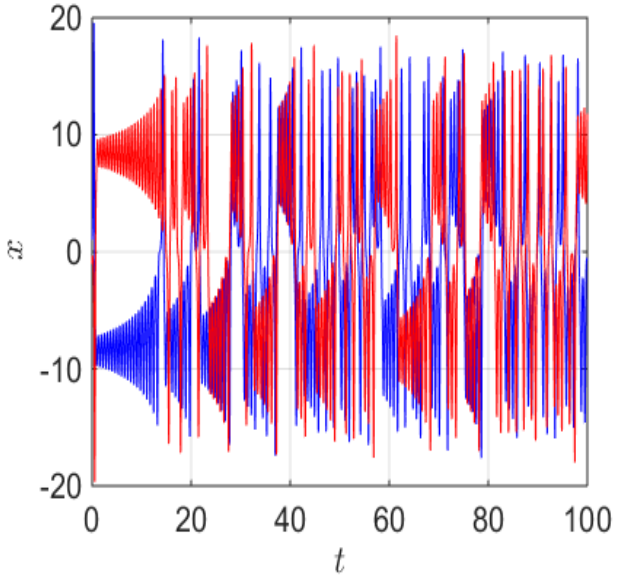


Figure 3.18: Time series of two points of the Lorenz system for $\rho = 28$.

### 3.4 Period doubling route to chaos

Chaotic attractors can happen in different ways in nonlinear dynamical systems. The four major routes to chaotic attractors are: period doubling cascade route, intermittency transition route, crisis route, and route to chaos in a quasi-periodically driven system. It has been observed that the Lorenz system undergoes a period doubling cascade route.

According to Poincaré, a period doubling bifurcation can be defined in a discrete dynamical system as a bifurcation in which the system switches to a new behavior with twice the period of the original system. Period doubling bifurcations can occur in continuous dynamical systems. They are observed in the Poincaré section. Assuming that a periodic orbit is created in a period doubling window, it generates a single point in the Poincaré section. If the orbit's characteristic multipliers become more negative than $-1$, then the new motion

remains periodic with a period twice the original motion's period. The period−two cycle may become unstable and give birth to a period−four cycle with four Poincaré intersection points.

A Poincaré section of $x = y$ is used to show period doubling bifurcation in the four period doubling windows found by Sparrow. The figures below show the phase portrait of the orbits for a value of $\rho$ at each periodic window in the left. Its trace in the Poincaré section of $x = y$ in the right hand side where the red dots represent the intersection of the orbits with the Poincaré section. The red points show where the period doublings occur.

The four period doubling windows investigated are:

- $99.5 < \rho < 100.86$

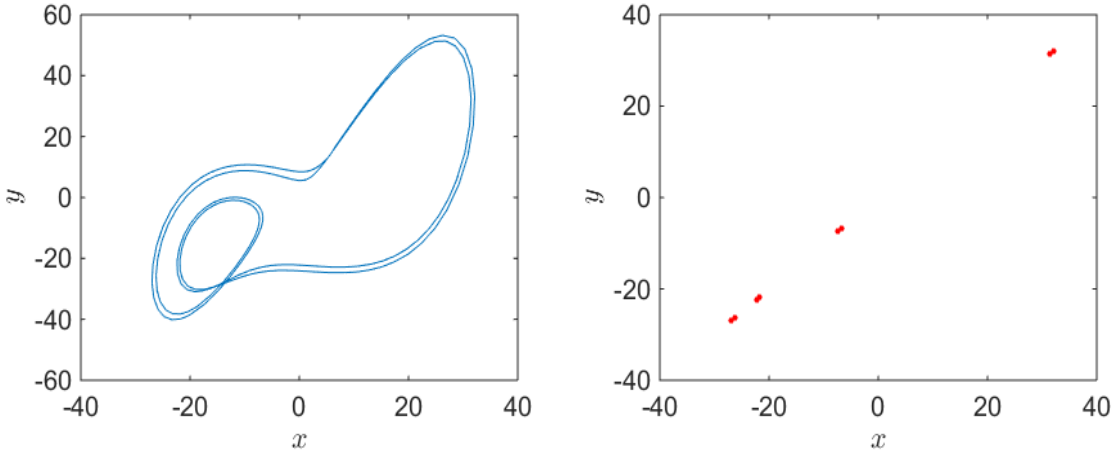


Figure 3.19: Lorenz system's phase portrait and its trace in the Poincaré map for $\rho = 100$

- $126.4 < \rho < 126.55$

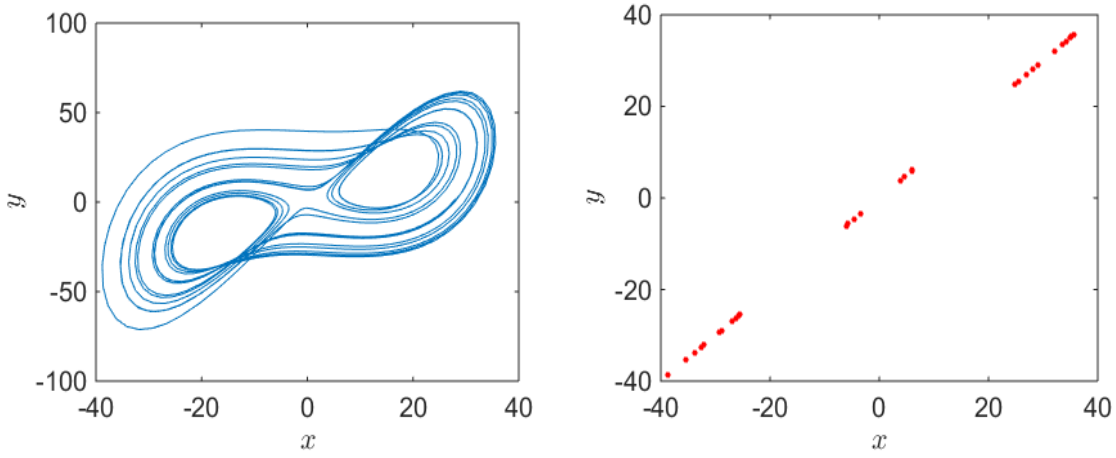


Figure 3.20: Lorenz system's phase portrait and its trace in the Poincaré map for $\rho = 126.5$

- $145 < \rho < 167$

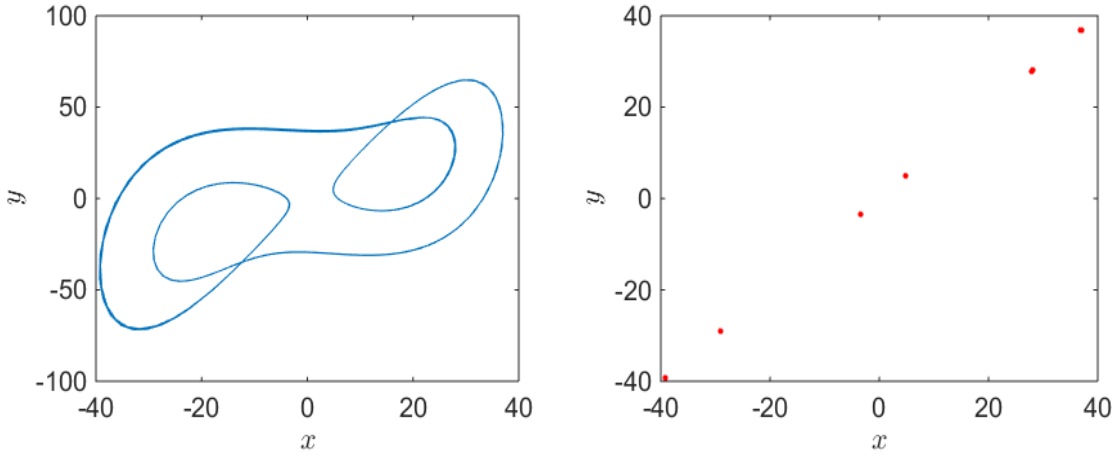


Figure 3.21: Lorenz system's phase portrait and its trace in the Poincaré map for $\rho = 150$

- $215 < \rho < 313$

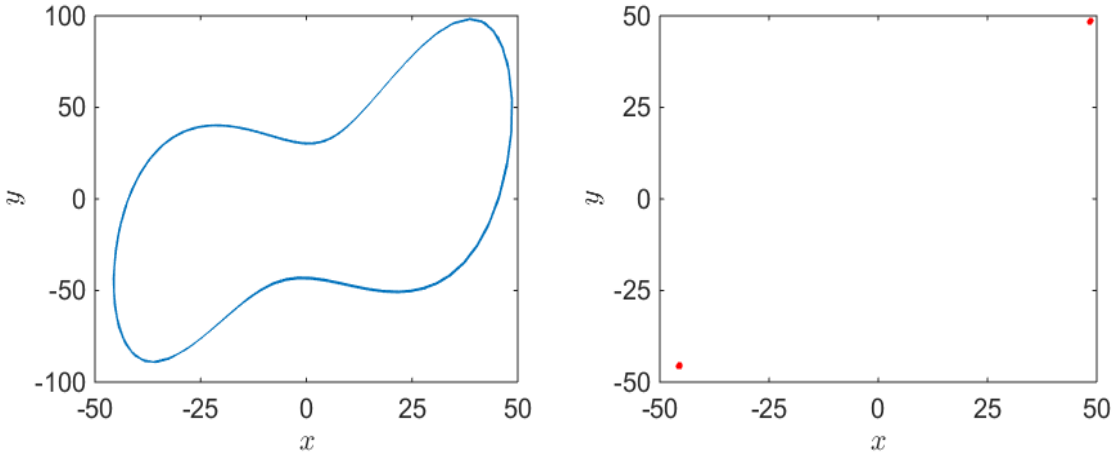


Figure 3.22: Lorenz system's phase portrait and its trace in the Poincaré map for $\rho = 305$

# CHAPTER IV

# SENSITIVITY ANALYSIS OF CHAOTIC SYSTEMS

## 4.1 Standard sensitivity analysis

In this thesis, standard sensitivity analysis methods are defined as direct (or forward) and adjoint sensitivity analysis. Direct and adjoint sensitivity analysis can be derived for the following nonlinear dynamical system represented by

$$\frac{d\boldsymbol{x}}{dt} = \boldsymbol{f}(\boldsymbol{x}, \alpha, t) \tag{4.1}$$

$$\boldsymbol{x}|_{t=0} = \boldsymbol{x}_0, \tag{4.2}$$

where $\boldsymbol{x} = \boldsymbol{x}(\alpha, t)$ is the state and $\alpha$ is a parameter with respect to which sensitivity of $\boldsymbol{x}$ is required. The differentiation of this equation with respect to $\alpha$ gives

$$\frac{d\boldsymbol{x}_\alpha}{dt} = \boldsymbol{J}\boldsymbol{x}_\alpha + \boldsymbol{f}_\alpha \tag{4.3}$$

$$\boldsymbol{x}_\alpha|_{t=0} = 0, \tag{4.4}$$

where $\boldsymbol{x}_\alpha = d\boldsymbol{x}/d\alpha$ is the sensitivity state, $J = \partial \boldsymbol{f}(\boldsymbol{x}, \alpha, t)/\partial \boldsymbol{x}$ is the Jacobian, and $\boldsymbol{f}_\alpha = \partial \boldsymbol{f}(\boldsymbol{x}, \alpha, t)/\partial \alpha$ is the sensitivity with respect to $\alpha$. Since the linearization is performed about a known state $\boldsymbol{x}$, the solution of Eq.(4.1)is required before Eq.(4.3) can be solved.

Engineers are interested in a time-averaged quantity given by

$$Q(\alpha) = \lim_{T\to\infty} \frac{1}{T} \int_0^T q(\boldsymbol{x}, \alpha, t) dt \tag{4.5}$$

where $q(\boldsymbol{x}, \alpha, t)$ is the instantaneous quantity of interest evaluated at time $t$. The limit on $T$ exists beacuse engineers are interested in an infinite averaging time. Computationally, the value of $T$ is chosen high enough to ensure the convergence of $Q(\alpha)$, which is when it does not change as $T$ varries.

The sensitivity of the time-averaged quantity with respect to $\alpha$ is defined as:

$$Q(\alpha)^q_\alpha = \frac{dQ(\alpha)}{d\alpha} = \lim_{T\to\infty} \frac{1}{T} \int_0^T \frac{dq(\boldsymbol{x}, \alpha, t)}{d\alpha} dt = \lim_{T\to\infty} \frac{1}{T} \int_0^T \frac{\partial q(\boldsymbol{x}, \alpha, t)}{\partial \alpha} + \frac{\partial q(\boldsymbol{x}, \alpha, t)^T}{\partial \boldsymbol{x}} \boldsymbol{x}_\alpha dt. \tag{4.6}$$

In order to evaluate $Q(\alpha)$ and $Q(\alpha)^q_\alpha$, convergence of the time-averaged quantity (and its derivative) for a finite time $T$ is required.

Eq.(4.6) defines the direct sensitivity analysis approach which necessitates the evaluation of $\boldsymbol{x}_\alpha$. In case the system has multiple parameters, Eq.(4.6) and Eq.(4.6) need to be solved for each parameter. This can be avoided using an adjoint approach by multiplying the governing equation Eq.(4.1), with a Lagrange multiplier, $\boldsymbol{l}$, and adding to the quantity-of-interest:

$$Q(\alpha) = \lim_{T\to\infty} \frac{1}{T} \int_0^T \left( q(\boldsymbol{x}, \alpha, t) + \boldsymbol{l}^T \left( \frac{d\boldsymbol{x}}{dt} - \boldsymbol{f}(\boldsymbol{x}, \alpha, t) \right) \right) dt. \tag{4.7}$$

Then, the adjoint sensitivity of time-averaged $Q(\alpha)$ is defined as

$$Q(\alpha)^q_\alpha = \lim_{T\to\infty}\frac{1}{T}\int_0^T \frac{\partial q(\boldsymbol{x},\alpha,t)}{\partial \alpha} + \frac{\partial q(\boldsymbol{x},\alpha,t)}{\partial \boldsymbol{x}}^T \boldsymbol{x}_\alpha \tag{4.8}$$

$$+ \boldsymbol{l}^T_\alpha(\frac{d\boldsymbol{x}}{dt} - \boldsymbol{f}(\boldsymbol{x},\alpha,t) + \boldsymbol{l}^T(\frac{d\boldsymbol{x}_\alpha}{dt} - \boldsymbol{f}_\alpha - \boldsymbol{J}\boldsymbol{x}_\alpha)dt \tag{4.9}$$

$$= \lim_{T\to\infty}\frac{1}{T}\int_0^T \left[\frac{\partial q(\boldsymbol{x},\alpha,t)}{\partial \alpha} + \boldsymbol{l}^T_\alpha\frac{d\boldsymbol{x}}{dt} + \left(\frac{\partial q(\boldsymbol{x},\alpha,t)}{\partial \alpha} - \boldsymbol{l}^T\boldsymbol{J}\right)\boldsymbol{x}_\alpha - \boldsymbol{l}^T\boldsymbol{f}_\alpha\right]dt \tag{4.10}$$

$$= \lim_{T\to\infty}\frac{1}{T}\int_0^T \left[\frac{\partial q(\boldsymbol{x},\alpha,t)}{\partial \alpha} + (\frac{\partial q(\boldsymbol{x},\alpha,t)}{\partial \boldsymbol{x}}^T - \frac{d\boldsymbol{l}^T}{dt} - \boldsymbol{l}^T\boldsymbol{J})\boldsymbol{x}_\alpha - \boldsymbol{l}^T\boldsymbol{f}_\alpha\right]dt + \boldsymbol{l}^T\boldsymbol{f}_\alpha|^{t=T}_{t=0} \tag{4.11}$$

where, the third term is dropped in Eq.(4.9) due to Eq.(4.1) and integration-by-parts is used on the second term in Eq.(4.10). Then, defining the adjoint problem as

$$\frac{d\boldsymbol{l}}{dt} = -\boldsymbol{J}^T\boldsymbol{l} + \frac{\partial q(\boldsymbol{x},\alpha,t)}{\partial \boldsymbol{x}} \tag{4.12}$$

$$\boldsymbol{l}|_{t=T} = 0, \tag{4.13}$$

simplifies the adjoint sensitivity Eq.(4.12) to

$$Q(\alpha)^q_\alpha = \lim_{T\to\infty}\frac{1}{T}\int_0^T \left[\frac{\partial q(\boldsymbol{x},\alpha,t)}{\partial \alpha} - \boldsymbol{l}^T\boldsymbol{f}_\alpha\right]dt. \tag{4.14}$$

Eq.(4.14) requires $\boldsymbol{l}$, which is obtained from the solution of Eq.(4.12). The adjoint equation is solved backwards in time with the initial condition defined at $t = T$, as in Eq.(4.13).

## 4.2 The problem of standard sensitivity analysis for chaotic systems

In chaotic systems, any small perturbation to the system will lead to momentous changes in the time accurate response of the system due to the Butterfly Effect. Even though the

nonlinearity of the system keeps the solution bounded, its linearized solution using standard sensitivity analysis methods will amplify or decay depending on the stability of the eigenvalues, eigenvectors of the Jacobian matrix $\mathbf{J}$, and the force function [14]. Applying direct and adjoint sensitivity analysis methods to time-averaged quantities result in an exponential growth of sensitivites as the averaging time $T$ increases causing round off errors and numerical overflow with finite precision arithmetic. Therefore, the sensitivities computed by the standard methods are not all that useful.

## 4.3 Multiprecision analysis

The solution of the nonlinear Lorenz system exhibits chaotic behavior but remains bounded unless an instability forces an unbounded growth of the solution. The objective is to investigate the sensitivity of time-averaged quantities obtained by the time accurate chaotic response of the Lorenz system. Analysis with arbitrary precision computations for chaotic sensitivity analysis of the Lorenz system is considered to study whether the sensitivity of the infinitely long time-average is converging or not.

### 4.3.1 Arbitrary-precision arithmetic

In computer science, arbitrary-precision arithmetic or bignum arithmetic indicates that the calculations are done on numbers that have high precision digits limited only by the system's available memory. Many modern programming languages have built-in support for bignums, and others have libraries available for arbitrary-precision integer and floating-point math [37]. Arbitrary precision is used in applications where precise results with very large numbers are required, and the speed of arithmetic is not a limiting factor.

### 4.3.2 Multi-precision Libraries

#### 4.3.2.1 GMP: GNU Multiple Precision

GNU Multiple Precision Arithmetic Library (GMP) is a library for arbitrary-precision arithmetic, used on signed integers, rational numbers, and floating point numbers. Their precision has no limit except the one implied by the machine's available memory [38]. GMP runs on:

- For 32-bit machines, dimension limit is $2^{32} - 1$ bits.
- For 64-bit machines, dimension limit is $2^{64} - 1$ bits.

GMP aims to be faster than any other bignum library for all operand sizes mainly by using different algorithms for different operand sizes; algorithms that are faster for very big numbers are usually slower for small numbers.

#### 4.3.2.2 MPFR: Multiple Precision Floating-Point Reliably

Based on GNU Multi-Precision Library, GNU MPFR (GNU Multiple Precision Floating-Point Reliably) is a GNU portable C library for arbitrary-precision binary floating-point computation with correct rounding [39]. The computation is efficient and has well-defined semantics. It provides support for special numbers: signed zeros $-0$, infinities and not$-$a$-$number where each number has its own precision. MPFR implements all mathematical functions: logarithm, exponential, trigonometric, hyperbolic functions, etc.

#### 4.3.2.3 Boost multi-precision

Boost is a set of libraries for the C++ programming language that provide support for linear algebra, pseudorandom number generation, multithreading, image processing,

regular expressions, multi-precision and unit testing, etc. Boost's multi-precision library provides extended precision arithmetic types for floating point, integer and rational arithmetic types in C++ that have more range and precision than C++'s ordinary built-in types [40]. Depending on the number type, precision can be arbitrarily large (limited only by the available memory), fixed at compile time (for example 50 or 100 decimal digits), or varied by member functions at run-time.

### 4.3.3 Methods

#### 4.3.3.1 Boost multi-precision methods

- Cpp bin float: It acts as an entirely C++ floating-point number type that is a drop-in replacement for the native C++ floating-point types, but with much greater precision. It provides arithmetic types at 50 and 100 decimal digits precision. This type has a radix of 2, even if the precision is specified as decimal digits.

- Cpp dec float: Precision can be specified to get arithmetic types at 50 and 100 decimal digits precision. The radix of this type is 10. As a result, it can behave slightly differently from base-2 types.

- Gmp float: It acts as a thin wrapper around the GMP to provide a real-number type. The type definitions provide arithmetic types at 50, 100, 500 and 1000 decimal digits precision.

### 4.3.4 Results

The sensitivity analysis of the time-averaged quantity of the time accurate response of the nonlinear Lorenz system was investigated (see Chapter 5 for more details). The multi-

precision arithmetic library Boost was able to provide arbitrary precised types using GMP to calculate the sensitivity of the time-averaged of the chaotic response of Lorenz system using the standard sensitivity analysis method.

However, as shown in Fig. 4.1 this quantity did not converge to a specific value for long time periods. Therefore an new approach to calculate the direct and adjoint sensitivity analysis of chaotic system will be followed.

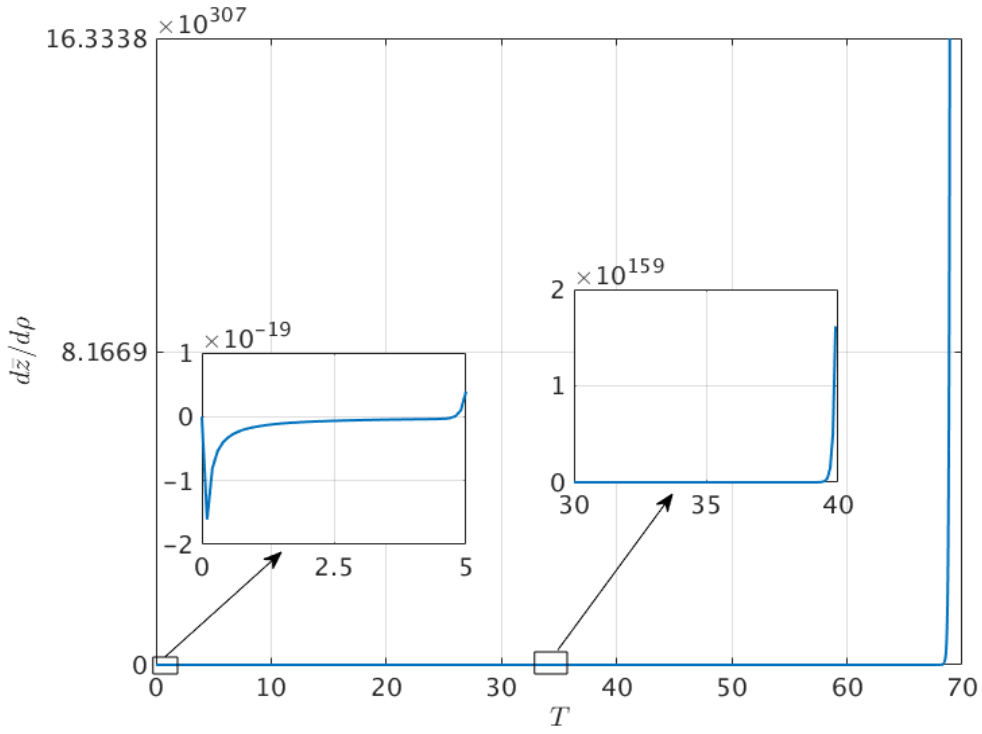


Figure 4.1: Sensitivity of $\bar{z}$ with respect $\rho$ using standard ODE solver with multipricision.

## 4.4 Current approach

The approach used in this thesis to obtain a stable and accurate sensitivity of the quantity-of-interest with respect to a parameter is discussed in a detailed manner by Bhatia and Makhija [14] where the requirements to compute time-accurate adjoint and direct sensitivity variables are relaxed.

### 4.4.1 Adaptive time-integration for sensitivity equations

Time-integration schemes are developed to solve the direct and adjoint problems. Discontinuous Galerkin finite element approach is used to derive a scheme where the time-step size can be adaptively chosen. Maintaining the stability of the linearized sensitivity problem is the primary criteria defined for selecting a time-step [14].

### 4.4.2 Update schemes

The recursive update scheme applied at each time step to solve for the direct sensitivity is

$$\boldsymbol{x}_{\alpha}^{1} = (\boldsymbol{I} - \boldsymbol{A}_1)^{-1}(\boldsymbol{x}_{\alpha}^{0} + \boldsymbol{F}_{\alpha}), \tag{4.15}$$

where

$$\boldsymbol{A}_1 = \int_{t_0^+}^{t_1^-} \boldsymbol{J} dt, \tag{4.16}$$

and

$$\boldsymbol{F}_{\alpha} = \int_{t_0^+}^{t_1^-} \boldsymbol{f}_{\alpha} dt. \tag{4.17}$$

This formula is the Backward-Euler scheme. Its stability is identified from the eigenvalues of the matrix $(\boldsymbol{I} - \boldsymbol{A}_1)^{-1}$ which are influenced by both: the length of the interval $t_1 - t_0$, and the change in $\boldsymbol{J}$ during this interval.

Adjoint equations are solved in reverse time and the recursive update scheme applied at each time step is

$$\boldsymbol{l}^0 = (\boldsymbol{I} + \boldsymbol{B}_0)^{-1}(\boldsymbol{l}^1 + \boldsymbol{G}) \tag{4.18}$$

where,

$$\boldsymbol{B}_0 = \int_{t_0^-}^{t_{-1}^+} \boldsymbol{J} dt, \tag{4.19}$$

and

$$\boldsymbol{G} = \int_{t_0^-}^{t_{-1}^+} \frac{\partial q(\boldsymbol{x}, \alpha, t)}{\partial \boldsymbol{x}} dt. \tag{4.20}$$

To solve for adjoint states $\boldsymbol{l}^0$, values from previous time step are required $\boldsymbol{l}^1$.

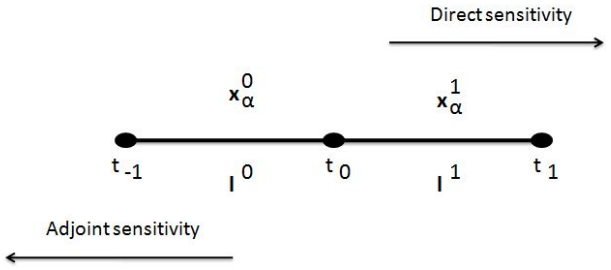


Figure 4.2: Two consecutive time intervals between $[t_{-1},t_0]$ with states $\boldsymbol{x}_\alpha^0$ and $\boldsymbol{x}_\alpha^1$ and adjoint states $\boldsymbol{l}^0$ and $\boldsymbol{l}^1$, respectively.

### 4.4.3 Norm-based time-step control

Given that the primary objective of the recursive update algorithm is to prevent unbounded growth of the sensitivity solution, an approximation to the amplification factor is defined as

$$\tilde{a} = \frac{||\boldsymbol{x}_\alpha^1||}{||\boldsymbol{x}_\alpha^0 + \boldsymbol{F}_\alpha||}. \tag{4.21}$$

The time integration scheme is stable when

$$\tilde{a} \leq \bar{a} \leq 1, \tag{4.22}$$

where, $\bar{a}$ is a predefined limit on the amplification factor. Both $\boldsymbol{x}^1$ and $t_1$ are unknowns and $t_1$ is adaptively identified to ensure stability. This approach always ensures decay of solution in accordance with the specified value for $\bar{a}$. The algorithm of this approach is presented by Bhatia and Makhija [14].

# CHAPTER V

# SENSITIVITY ANALYSIS OF LORENZ SYSTEM

In this chapter a sensitivity analysis study on Lorenz system is presented. As seen in Chapter 3, Lorenz system is a nonlinear ODE that can exhibit chaotic responses such as strange attractor, limit cycle oscillations, and period doubling cascades depending on the values of $\rho$. The system is defined as

$$\frac{d\boldsymbol{x}}{dt} = \boldsymbol{f}(\boldsymbol{x}, \sigma, \rho, \beta, t) \tag{5.1}$$

$$\boldsymbol{x}|_{t=0} = \boldsymbol{x}_0, \tag{5.2}$$

where,

$$\boldsymbol{x} = \begin{bmatrix} x \\ y \\ z \end{bmatrix} \tag{5.3}$$

and

$$\boldsymbol{f} = \begin{bmatrix} \sigma(y - x) \\ x(\rho - z) - y \\ xy - \beta z \end{bmatrix} \tag{5.4}$$

and $\rho$ is the parameter with respect to which sensitivity of $(x)$ is considered. Differentiation of the governing equation with respect to $\rho$ gives

$$\frac{d\boldsymbol{x}_\rho}{dt} = \boldsymbol{f}_\rho + \boldsymbol{J}\boldsymbol{x}_\rho \tag{5.5}$$

where

$$\boldsymbol{J} = \frac{\partial \boldsymbol{f}}{\partial \boldsymbol{x}} = \begin{bmatrix} -\sigma & \sigma & 0 \\ \rho & -1 & -x \\ y & x & -\beta \end{bmatrix} \tag{5.6}$$

and

$$\boldsymbol{f}_\rho = \frac{\partial \boldsymbol{f}}{\partial \rho} = \begin{bmatrix} 0 \\ x \\ 0 \end{bmatrix} \tag{5.7}$$

The time-averaged $z$ and $z^2$ are given by

$$Q^z = \bar{z} = \lim_{T\to\infty} \frac{1}{T} \int_0^T z dt \tag{5.8}$$

$$Q^{z^2} = \bar{z^2} = \lim_{T\to\infty} \frac{1}{T} \int_0^T z^2 dt \tag{5.9}$$

and their sensitivities

$$Q^z_\rho = \bar{z}_\rho = \lim_{T\to\infty} \frac{1}{T} \int_0^T \frac{dz(t)}{d\rho} dt \tag{5.10}$$

$$Q^{z^2}_\rho = \bar{z^2}_\rho = \lim_{T\to\infty} \frac{1}{T} \int_0^T \frac{dz(t)^2}{d\rho} dt \tag{5.11}$$

The values of time-averaged quantities $\bar{z}$ and $\bar{z^2}$ are computed for 8 different initial conditions at each $\rho$ using an averaging time of $T = 1000s$. 200 uniformly spaced values

of $\rho$ between $[1, 200]$ are used and Fig. 5.1(b) and Fig. 5.2(b) show the values of $\bar{z}$ and $\bar{z^2}$ respectively, plotted versus $\rho$. A least-squares regression approach is used to estimate the slopes of both $\bar{z}$ and $\bar{z^2}$ versus $\rho$ in 20 uniformly spaced intervals of $\rho$ and are shown in Fig. 5.1(c) and Fig. 5.2(c). In the interval of $\rho \in [20, 25]$ The regression values of both $\bar{z}$ and $\bar{z^2}$ in Fig. 5.1(c) and Fig. 5.2(c) show a jump due to the occurence of the Lorenz attractor. Moreover as $\rho$ increases from $100$ to $200$, the chaotic system undergoes a period doubling cascade which leads to jumps in the estimated sensitivity values seen in Fig. 5.2(c).

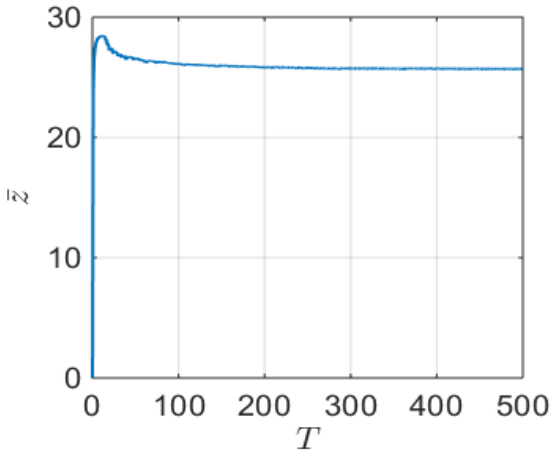


(a) Convergence of $\bar{z}$, $\rho = 30$

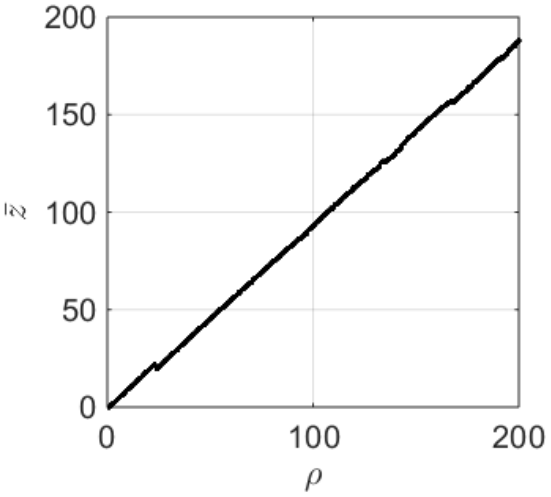


(b) time-averaged $\bar{z}$

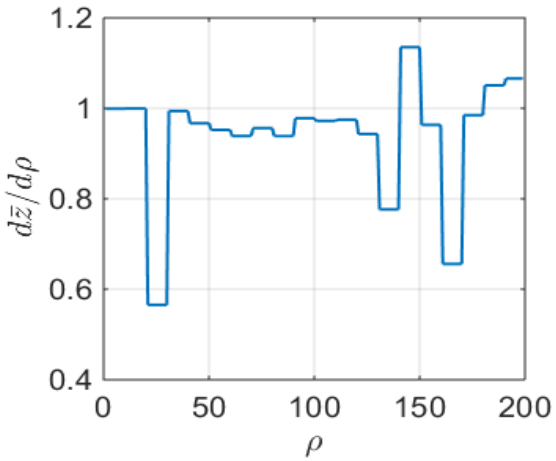


(c) Regression of $d\bar{z}/d\rho$

Figure 5.1: Time-averaged quantity $\bar{z}$ and its sensitivity $d\bar{z}/d\rho$.

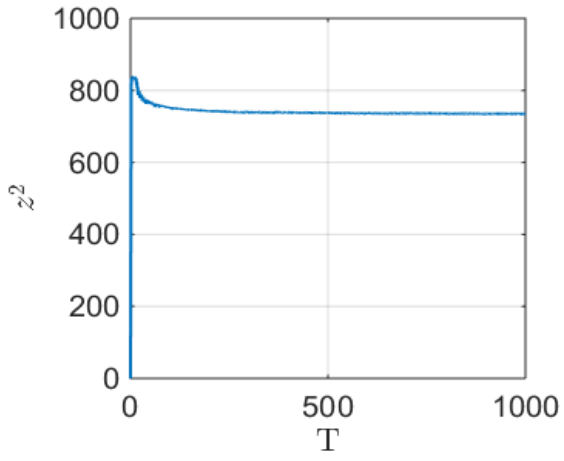


(a) Convergence of $\bar{z^2}$, $\rho = 30$

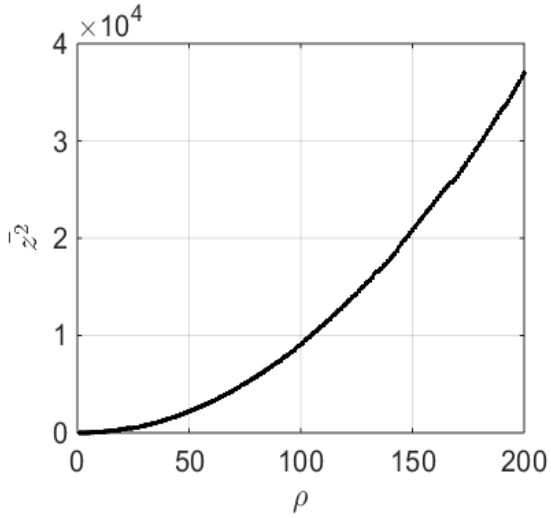


(b) time-averaged $\bar{z^2}$

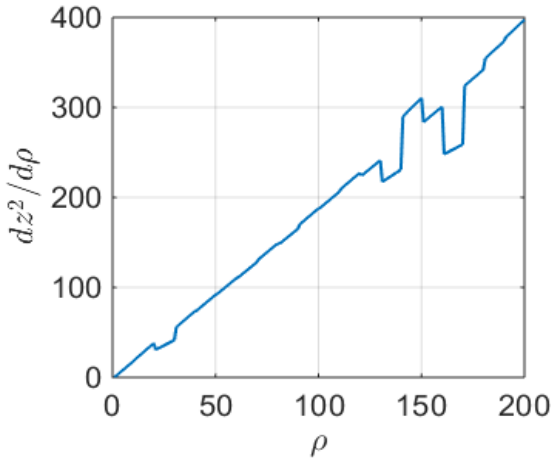


(c) Regression of $d\bar{z^2}/d\rho$

Figure 5.2: Time-averaged quantity $\bar{z}^2$ and its sensitivity $d\bar{z^2}/d\rho$.

A standard linear central difference ODE solver is used to calculate the time-accurate solution of the sensitivity problem at $\rho = 30$ with $dt = 10^{-2}s$. Sensitivities of $z$ and $z^2$ are plotted in Fig. 5.3(a) and Fig. 5.4(a) where the values oscillate and grow to order

$10^2$ for $z^2$, these values continue to grow by several orders of magnitude for longer time periods. Using the stabilized solver developed by Bhatia and Makhija [14], the direct and adjoint sensitivities remain bounded to smaller values during the simulation presented in Fig. 5.3(b) and Fig. 5.4(b) and Fig. 5.3(c) and Fig. 5.3(c) and show convergence for increasing averaging time for both quantities at hand.

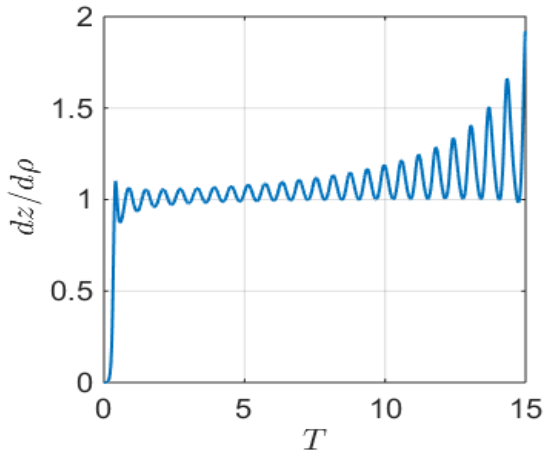


(a) Sensitivity with standard ODE solver

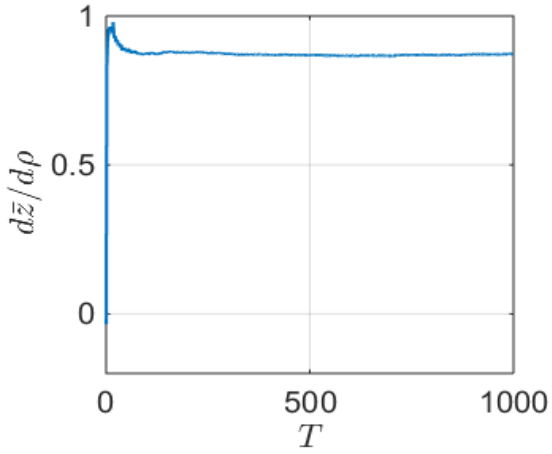


(b) Direct sensitivity

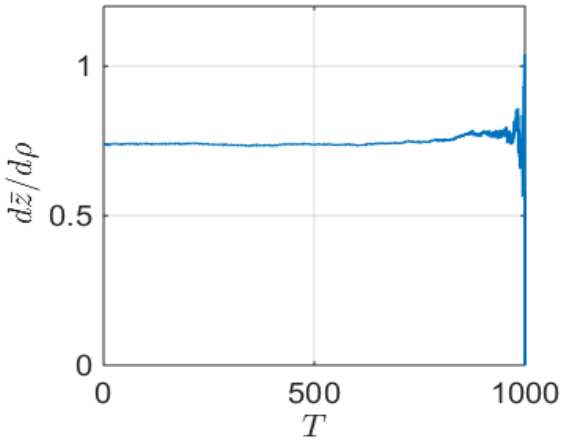


(c) Adjoint sensitivity

Figure 5.3: Sensitivity convergence of $d\bar{z}/d\rho$ at $\rho = 30$.

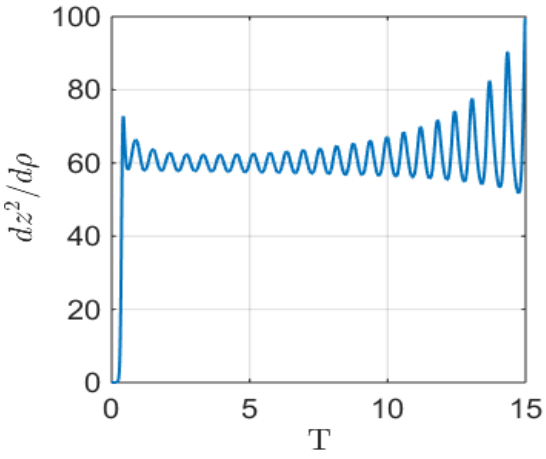


(a) Sensitivity with standard ODE solver

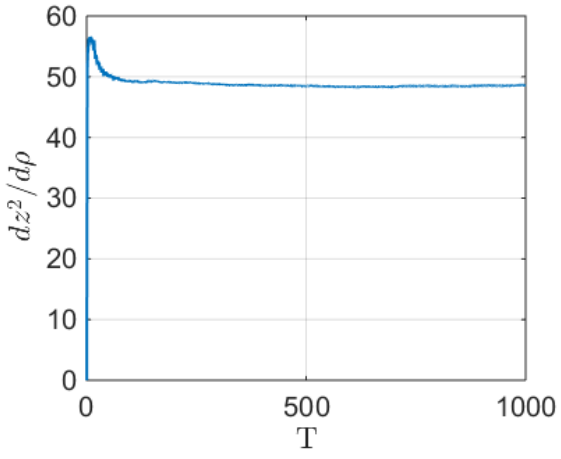


(b) Direct sensitivity

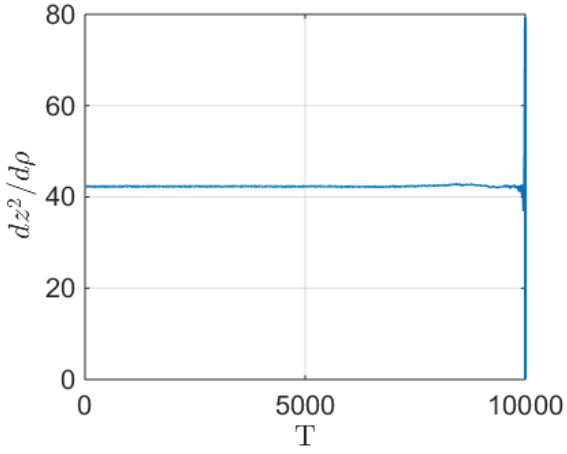


(c) Adjoint sensitivity

Figure 5.4: Sensitivity convergence of $d\bar{z^2}/d\rho$ at $\rho = 30$.

The adjoint problem is solved backward in time, therefore the sensitivity values start from zero at the respective time and increase towards $t = 0$. This is an important distinction

between the direct and adjoint approaches. Direct sensitivity solves the problem in forward time and allows a control on termination of the time integration whereas the adjoint method solves the problem backward in time and requires integration from final time to $t = 0$ before the the time-averaged adjoint sensitivity can be used.

Different values of amplification factor have been used to study the influence of $\bar{a}$ on the convergence of sensitivities of time-averaged quantities. In Fig. 5.5 and Fig. 5.6 the values of $d\bar{z}/d\rho$ and $d\bar{z}^2/d\rho$ are computed for $100$ uniformly spaced values of $\rho \in [1, 200]$ with 8 different initial conditions at each $\rho$. The initial values assume $x = z = 0.75$ and the value of $y$ is chosen at uniform intervals in $[-1, 1.1]$. An averaging duration of $T = 1000s$ is used for all results with $dt = 0,01s$ an $10,000$ time-steps for the nonlinear solver. It can be observed from the two figures Fig. 5.5and Fig. 5.5 that for $\bar{a} = 1$ the results show close agreement with the regression data for both direct and adjoint approaches. However, as the amplification factor decreases, the accuracy of the sensitivity results reduces and a larger spread in the range of $\rho \geq 130$ is seen.

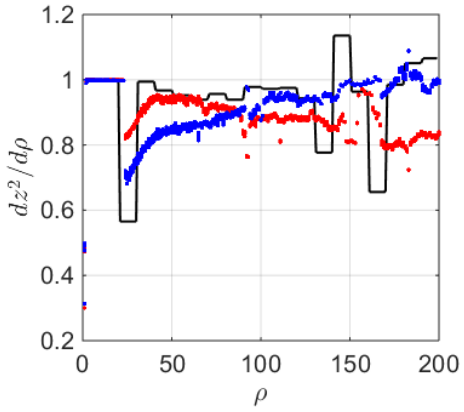


(a) $\bar{a} = 1$

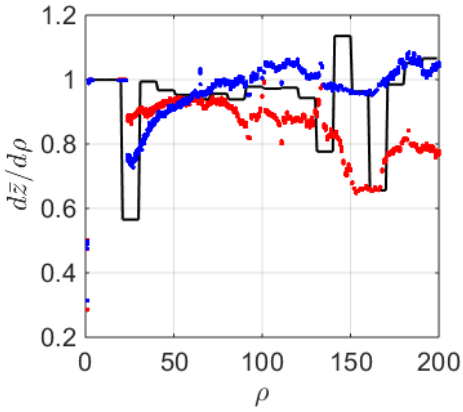


(b) $\bar{a} = 0.9$

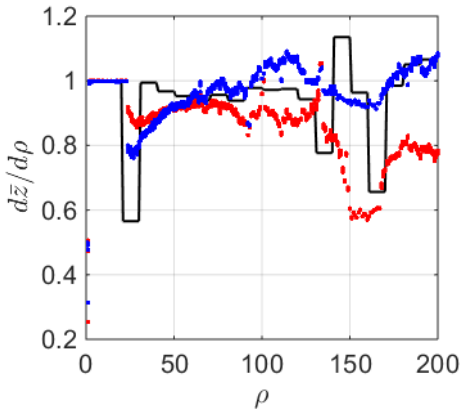


(c) $\bar{a} = 0.8$

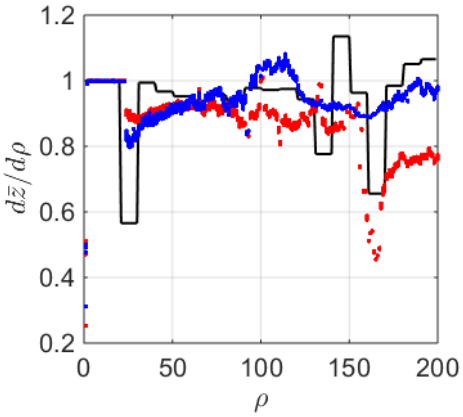


(d) $\bar{a} = 0.7$

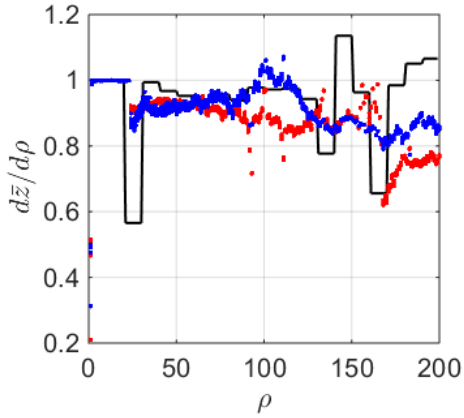


(e) $\bar{a} = 0.6$

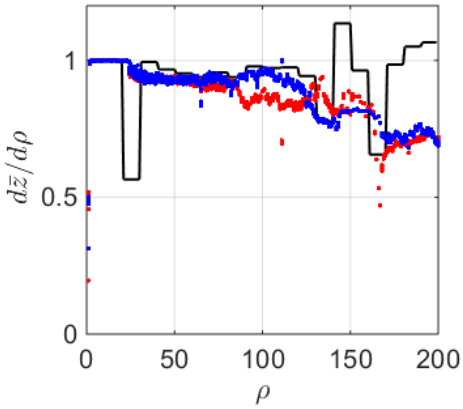


(f) $\bar{a} = 0.5$

Figure 5.5: Direct and adjoint sensitivities $d\bar{z}/d\rho$ for different amplification factors.

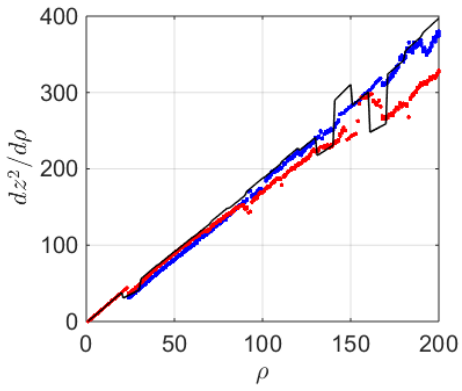


(a) $\bar{a} = 1$

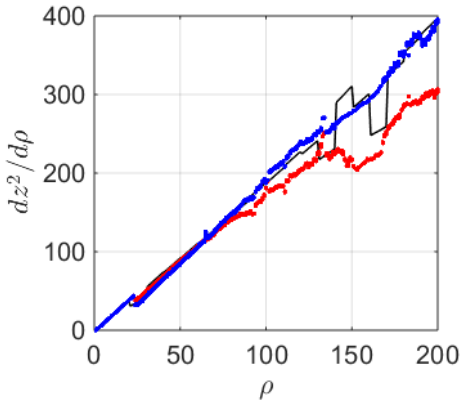


(b) $\bar{a} = 0.9$

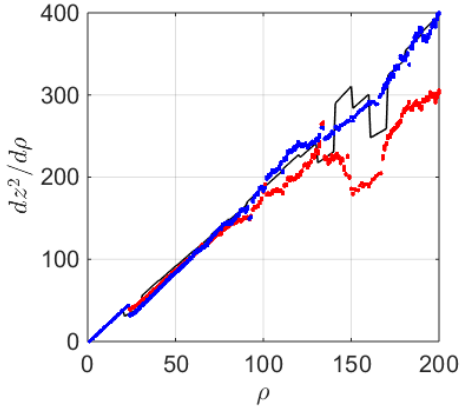


(c) $\bar{a} = 0.8$

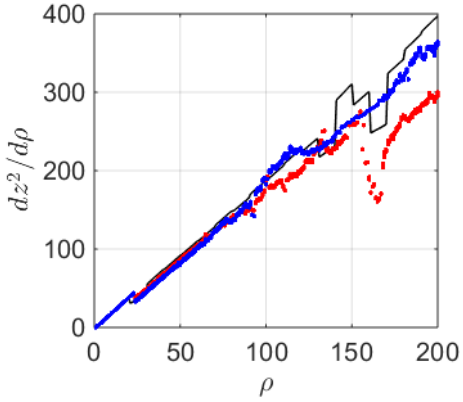


(d) $\bar{a} = 0.7$

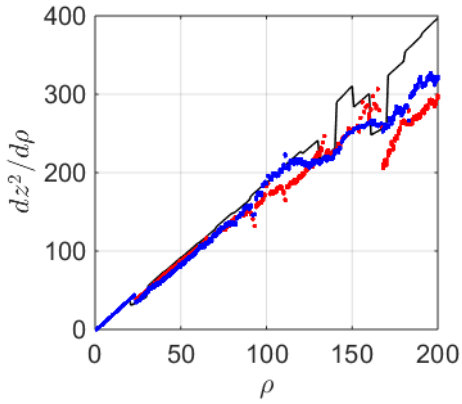


(e) $\bar{a} = 0.6$

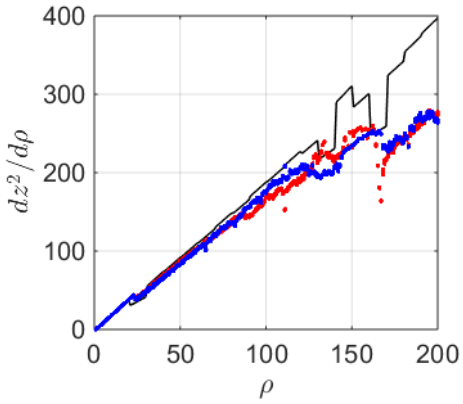


(f) $\bar{a} = 0.5$

Figure 5.6: Direct and adjoint sensitivities $d\bar{z^2}/d\rho$ for different amplification factors.

It can be observed that different results are obtained using the direct and adjoint sensitivity analyses for the same cases. This is due to the fact that the stabilization solver chooses time-step size independently for each sensitivity solution. Moreover, The adjoint sensitivity results are in closer agreement with the regression data than those from the direct sensitivity.

The impact of averaging time, T, on the accuracy and convergence of the sensitivity quantities is studied for $dt = 0.01s$. Three different values of $\bar{a} = 0.6, 0.8, 1$ are studied and results are shown in Fig. 5.7and Fig. 5.8 for $\bar{z}$ and $\bar{z^2}$ respectively. This shows that as the averaging time increases, the direct and adjoint method are producing sensitivity values, $d\bar{z}/d\rho$ and $d\bar{z}^2/d\rho$, that are independent of the initial condition. However, the final values are seen to depend on the choice of $\bar{a}$ for both time-averaged quantities.

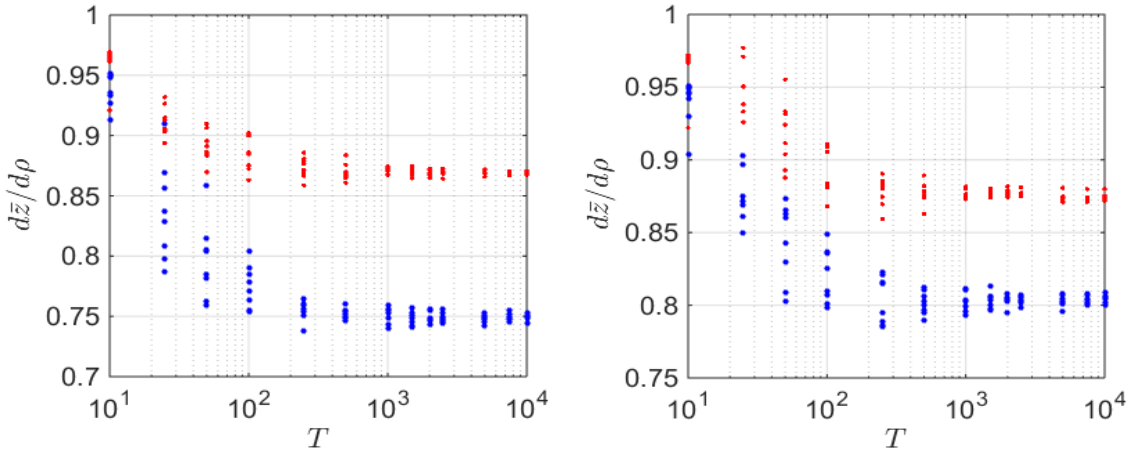


(a) $\bar{a} = 1$




(b) $\bar{a} = 0.8$

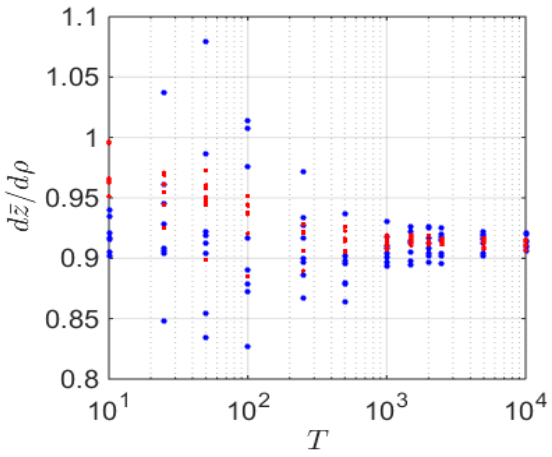


(c) $\bar{a} = 0.6$

Figure 5.7: Convergence of sensitivities $d\bar{z}/d\rho$ for different amplification factors at $\rho = 30$.

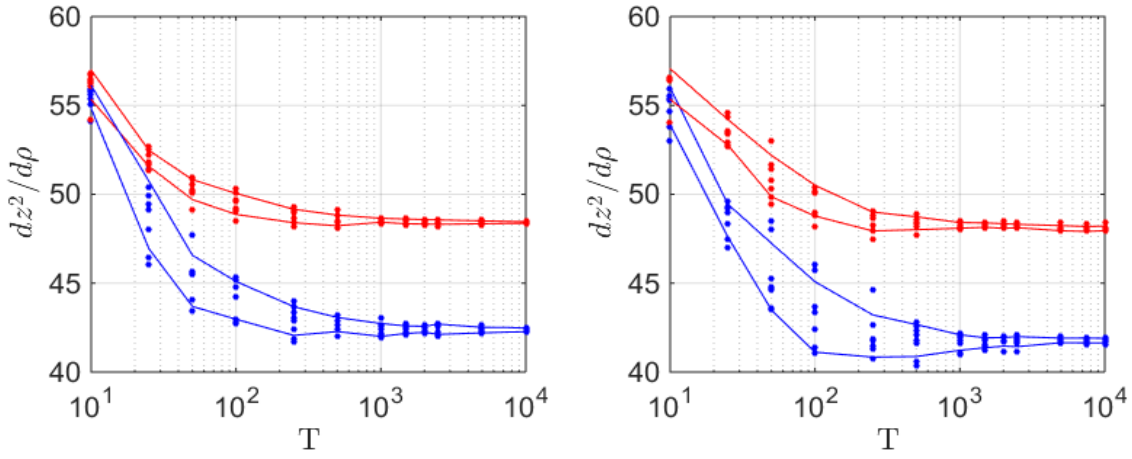


(a) $\bar{a} = 1$ (b) $\bar{a} = 0.8$

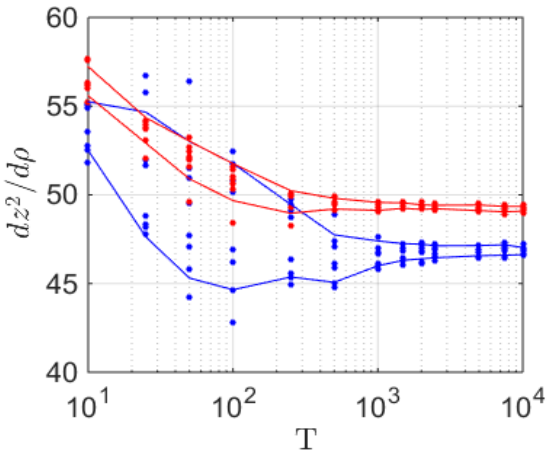


(c) $\bar{a} = 0.6$

Figure 5.8: Convergence of sensitivities $d\bar{z^2}/d\rho$ for different amplification factors at $\rho = 30$.

To quantify the convergence of the time-averaged quantities and their sensitivity, a measure has been introduced as $\sigma(Q(\alpha))/mean(Q(\alpha))$ and is presented in Fig. 5.9 and

Fig. **??** for both $\bar{z}$, $\bar{z^2}$ and their respective direct and adjoint sensitivities $d\bar{z}/d\rho$ and $d\bar{z^2}/d\rho$ at $\rho = 30$ for increasing averaging time.

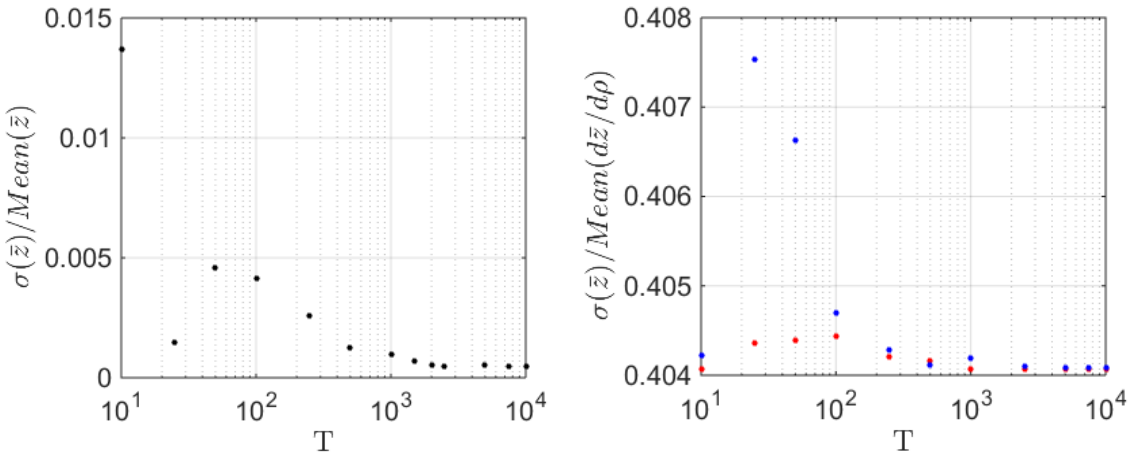


(a) Convergence of $z$

(b) Convergence of $d\bar{z}/d\rho$

Figure 5.9: Convergence of $z$ and its direct and adjoint sensitivities at $\rho = 30$ and $\bar{a} = 1$.

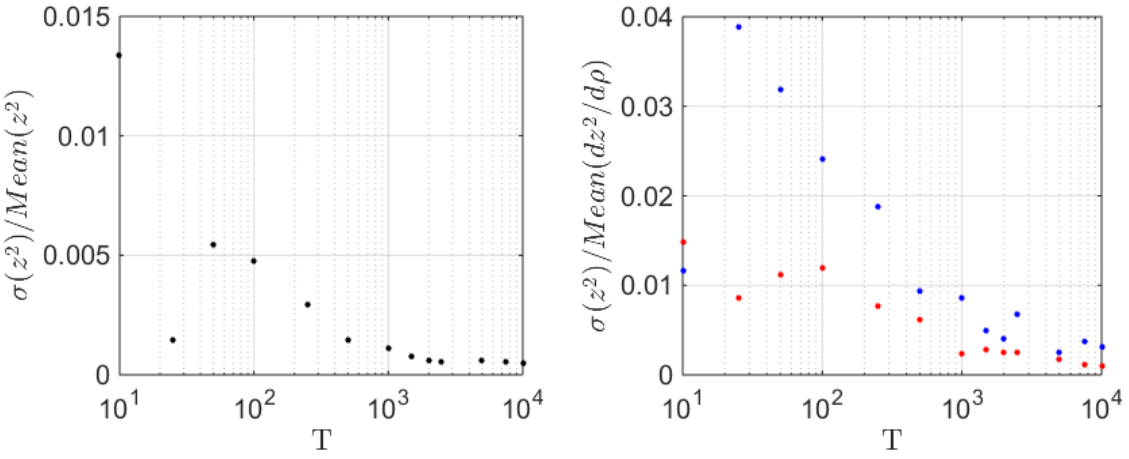


(a) Convergence of $z^2$

(b) Convergence of $d\bar{z^2}/d\rho$

Figure 5.10: Convergence of $z^2$ and its direct and adjoint sensitivities at $\rho = 30$ and $\bar{a} = 1$.

Both figures show that even though time-averaged $\bar{z}$ and $\bar{z^2}$ show similar convergence, the difference of convergence between their sensitivities $d\bar{z}/d\rho$ and $d\bar{z^2}/d\rho$ in the other hand is significant; using an averaging time of $T = 10^3$ to compute the sensitivity of $\bar{z}$ will give higher spread of its sensitivity values compared to the ones of $\bar{z^2}$ using the same averaging time. Which suggests that with the same number of iterations, direct and adjoint sensitivities of $\bar{z^2}$ will converge to a value that is independent of the initial condition.

# CHAPTER VI

# SENSITIVITY ANALYSIS OF DOUBLE PENDULUM

## 6.1 Governing equations of double pendulum system

Many important applications in engineering sciences have dynamical systems with pendulum elements. For instance, a study on double pendulum is important to control and optimize double arm robots [36]. Even though the response of a single mass pendulum is easily obtained, when combining two pendulums this simple dynamic system exhibits a complicated motion and the systems becomes very sensitive to initial conditions and its response turns out to be chaotic.

The schematic sketch of the double pendulum system considered in this paper is presented in Fig. 6.1. The the top pendulum is attached to a fixed point while its lower end is connected with the top end of the second pendulum. The arm of each pendulum is assumed to be massless. The solid sphere at the end pf each pendulum is the concentrated mass. Further $m_1$, $m_2$, $l_1$, $l_2$, $\theta_1$ and $\theta_2$ are the mass, length and angular displacement of the top and bottom pendulum respectively.

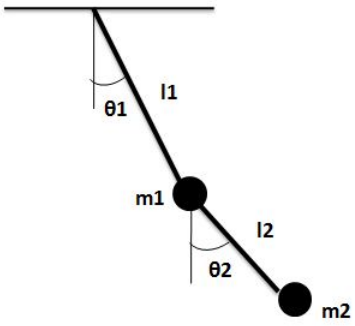


Figure 6.1: Schematic sketch of double pendulum.

The system of equations of the double pendulum can be derived using the positions of mass 1 and 2 given by

$$x_1 = l_1 \sin\theta_1 \tag{6.1}$$

$$y_1 = -l_1 \cos\theta_1 \tag{6.2}$$

$$x_2 = l_1 \sin\theta_1 + l_2 \sin\theta_2 \tag{6.3}$$

$$y_2 = -l_1 \cos\theta_1 - l_2 \cos\theta_2 \tag{6.4}$$

The corresponding angular velocities are

$$\dot{x}_1 = l_1 \cos\theta_1 \dot{\theta_1} \tag{6.5}$$

$$\dot{y}_1 = l_1 \sin\theta_1 \dot{\theta_1} \tag{6.6}$$

$$\dot{x}_2 = l_1 \cos\theta_1 \dot{\theta_1} + l_2 \cos\theta_2 \dot{\theta_2} \tag{6.7}$$

$$\dot{y}_2 = l_1 sin\theta_1 \dot{\theta_1} + l_2 sin\theta_2 \dot{\theta_2} \tag{6.8}$$

The kinetic energy $K$ and potential energy $P$ of the double pendulum is given by

$$K = \frac{1}{2}mv^2 \tag{6.9}$$

$$= \frac{1}{2}m(\dot{x}^2 + \dot{y}^2) \tag{6.10}$$

$$= \frac{1}{2}m_1(\dot{x_1}^2 + \dot{y_1}^2) + \frac{1}{2}m_2(\dot{x_2}^2 + \dot{y_2}^2) \tag{6.11}$$

$$= \frac{1}{2}(m_1 + m_2)l_1^2\dot{\theta_1}^2 + \frac{1}{2}m_2\dot{l_2}^2\dot{\theta_2}^2 + m_2 l_1 l_2 \theta_1 \theta_2 \cos(\theta_1 - \theta_2) \tag{6.12}$$

and

$$P = m_1 g y_1 + m_2 g y_2 \tag{6.13}$$

$$= -(m_1 + m_2)g l_1 \cos\theta_1 - m_2 g l_2 \cos(\theta_2) \tag{6.14}$$

The Hamiltonian of the system is

$$H = K + P \tag{6.15}$$

$$= \frac{1}{2}(m_1 + m_2)l_1^2\dot{\theta_1}^2 + \frac{1}{2}m_2\dot{l_2}^2\dot{\theta_2}^2 + m_2 l_1 l_2 \theta_1 \theta_2 \cos(\theta_1 - \theta_2) \tag{6.16}$$

$$- (m_1 + m_2)g l_1 \cos\theta_1 - m_2 g l_2 \cos(\theta_2) \tag{6.17}$$

The Lagrangian is then obtained as

$$L = K - P \tag{6.18}$$

$$= \frac{1}{2}(m_1 + m_2)l_1^2\dot{\theta_1}^2 + \frac{1}{2}m_2\dot{l_2}^2\dot{\theta_2}^2 + m_2 l_1 l_2 \theta_1 \theta_2 \cos(\theta_1 - \theta_2) \tag{6.19}$$

$$+ (m_1 + m_2)g l_1 \cos\theta_1 + m_2 g l_2 \cos(\theta_2) \tag{6.20}$$

For the Lagrangian of a system this Euler-Lagrange differential equation must be true

$$\frac{d}{dt}\left(\frac{\partial L}{\partial \dot{\theta}}\right) - \frac{\partial L}{\partial \theta} = 0 \tag{6.21}$$

A couple of algebraic manipulations yields the nonlinear system of equations of the double pendulum

$$\frac{d\mathbf{z}}{dt} = \mathbf{f}(\mathbf{z}, m_1, l_1, m_2, l_2, t) \tag{6.22}$$

where,

$$\mathbf{z} = \begin{bmatrix} \theta_1 \\ \theta_2 \\ \dot{\theta_1} \\ \dot{\theta_2} \end{bmatrix} \tag{6.23}$$

and

$$\mathbf{f} = \begin{bmatrix} \dot{\theta_1} \\ \dot{\theta_2} \\ \frac{-g(2m_1+m_2)\sin\theta_1 - gm_2\sin(\theta_1-2\theta_1) - 2m_2 l_2 \dot{\theta_2}^2 \sin(\theta_1-\theta_1) - 2m_1 l_1 \dot{\theta_1}^2 \cos(\theta_1-\theta_2)\sin(\theta_1-\theta_2)}{l_1 2m_1 + l_1 m_2 - l_1 m_2 \cos(2\theta_1 - 2\theta_2)} \\ \frac{\left(2l_1(m_1+m_2)\dot{\theta_1}^2 + 2g(m_1+m_2)\cos\theta_1 + l_2 m_2 \dot{\theta_2}^2 2\cos(\theta_1-\theta_2)\right)\sin(\theta_1-\theta_2)}{l_2 2m_1 + l_2 m_2 - l_2 m_2 \cos(2\theta_1 - 2\theta_2)} \end{bmatrix} \tag{6.24}$$

## 6.2 Time simulation of double pendulum system

It has been shown experimentally [34] and numerically [35] that the double pendulum exhibits periodic, quasi-periodic and chaotic behavior depending on the initial conditions of the system. The periodic behavior of the double pendulum during $t = 6s$ is observed in Fig. 6.2 where $\theta_1$ and $\theta_2$ presented in Fig. 6.2(a) are in phase and both pendulums are oscillating periodically around equilibrium point $x_1 = x_2 = 0$ Fig. 6.2 (b). Fig. 6.3 shows the quasi-periodic behavior of the system where the angles are no longer in phase and the

motion of the seco nd pendulum is quasi-periodic. The chaotic behavior of the system is shown in Fig. 6.4 where the motion of the second pendulum is random and unpredictable.

Time series of both angles $\theta_1$ and $\theta_2$ are presented in Fig. 6.2 for $m2 = 0.01$ shows the $x$ positions of the two masses $m_1$ and $m_2$ with respect to $y$.

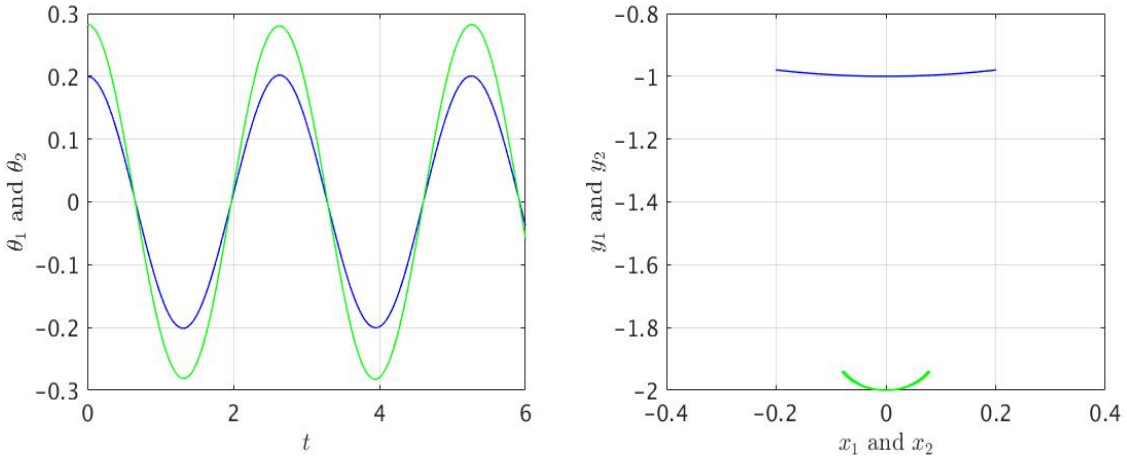


(a) Time series of angles $\theta_1$ and $\theta_2$

(b) Positions of $m_1$ and $m_2$ over time

Figure 6.2: Periodic behavior of double pendulum.

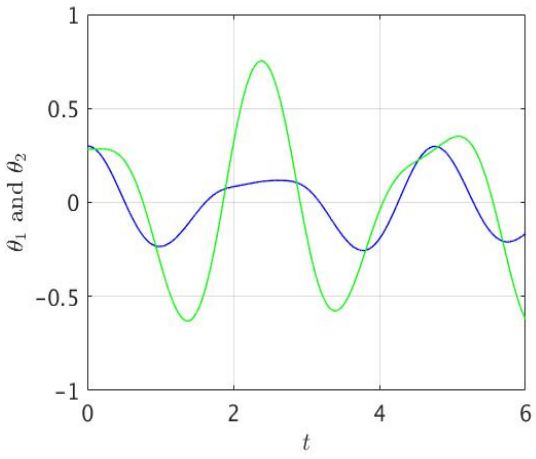


(a) Time series of angles $\theta_1$ and $\theta_2$

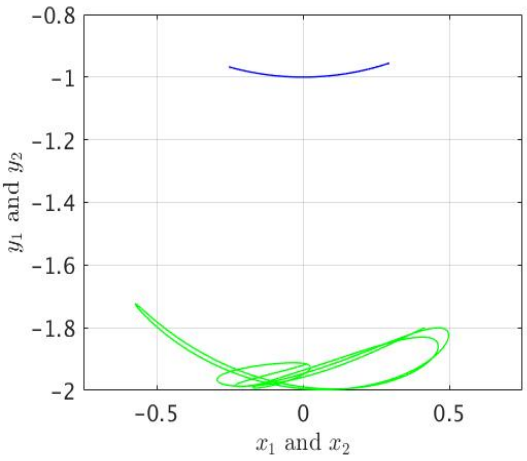


(b) Positions of $m_1$ and $m_2$ over time

Figure 6.3: Quasi periodic behavior of double pendulum.

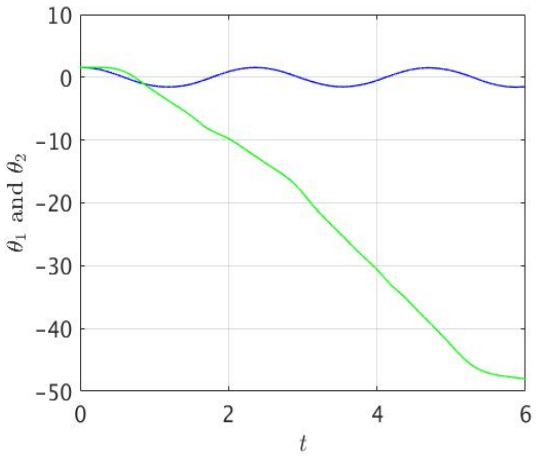


(a) Time series of angles $\theta_1$ and $\theta_2$

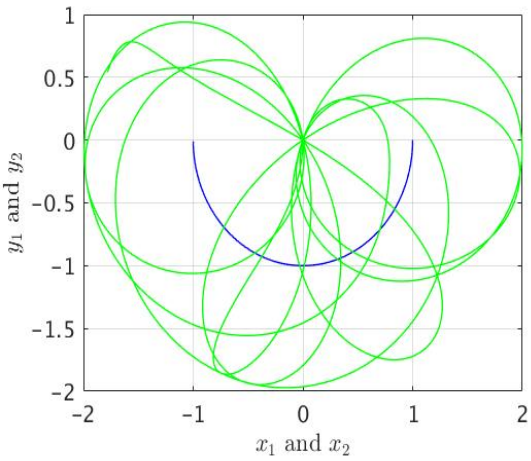


(b) Positions of $m_1$ and $m_2$ over time

Figure 6.4: Chaotic behavior of double pendulum.

## 6.3 Sensitivity analysis of double pendulum

$m_2$ is the parameter with respect to which sensitivity of $(z)$ is considered. Differentiation of the governing equation with respect to $m_2$ gives:

$$\frac{\partial}{\partial m_2}\left(\frac{d\mathbf{z}}{dt}\right) = \frac{\partial}{\partial m_2}\left(\mathbf{f}(\mathbf{z}, m_2, t)\right) = \frac{\partial \mathbf{f}}{\partial m_2} + \frac{\partial \mathbf{f}}{\partial \mathbf{z}}\frac{\partial \mathbf{z}}{\partial m_2} \tag{6.25}$$

which becomes

$$\frac{d\mathbf{z}_{m_2}}{dt} = \mathbf{f}_{m_2} + \mathbf{J}\mathbf{z}_{m_2} \tag{6.26}$$

The two quantities of interest are the time-averaged position $x_2$ and its square $x_2^2$ which are obtained by

$$Q^{x_2} = \bar{x_2} = \lim_{T\to\infty}\frac{1}{T}\int_0^T x_2 dt \tag{6.27}$$

$$Q^{x_2^2} = \bar{x_2^2} = \lim_{T\to\infty}\frac{1}{T}\int_0^T x_2^2 dt \tag{6.28}$$

and their sensitivities

$$Q^{x_2}_{m_2} = \bar{x_2}_{m_2} = \lim_{T\to\infty}\frac{1}{T}\int_0^T \frac{dx_2(t)}{dm_2} dt \tag{6.29}$$

$$Q^{x_2^2}_{m_2} = \bar{x_2^2}_{m_2} = \lim_{T\to\infty}\frac{1}{T}\int_0^T \frac{dx_2(t)^2}{dm_2} dt \tag{6.30}$$

The values of time-averaged quantities $\bar{x_2}$ and $\bar{x_2^2}$ are computed for 8 different initial conditions at each $m2$ using an averaging time of $T = 1000s$. 50 uniformly spaced values of $m_2$ between $[0.1, 6]$ are used and Fig. 6.5(b) and Fig. 6.6(b) show the values of $\bar{x_2}$ and $\bar{x_2^2}$ respectively, plotted versus $m_2$.

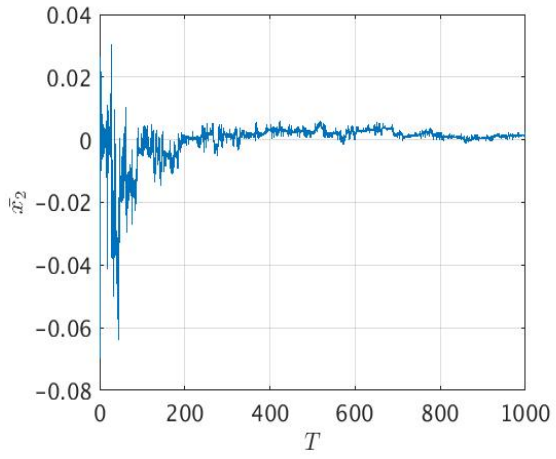


(a) Convergence of $\bar{x_2}$ at $m_2 = 4$

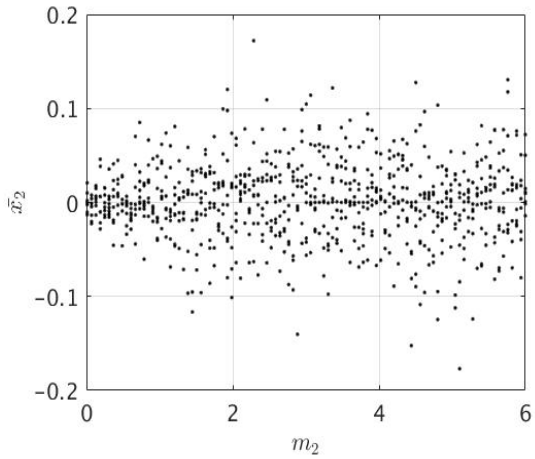


(b) time-averaged $\bar{x_2}$

Figure 6.5: Convergence of time-averaged quantity $\bar{x_2}$.

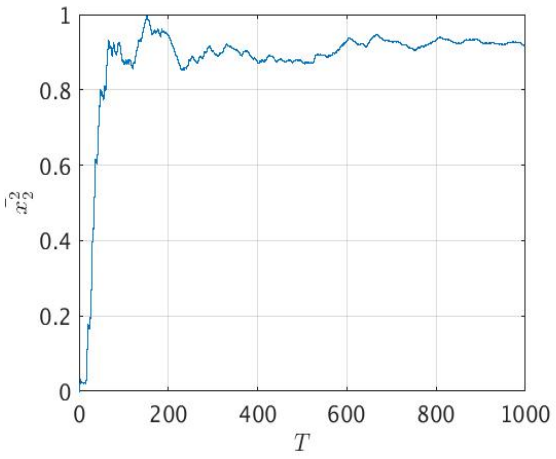


(a) Convergence of $\bar{x_2^2}$ at $m_2 = 4$

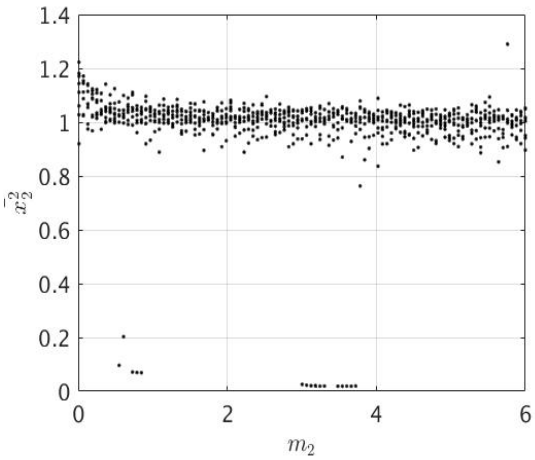


(b) time-averaged $\bar{x_2^2}$

Figure 6.6: Convergence of time-averaged quantity $\bar{x_2^2}$.

Time-averaged quantities $\bar{x_2}$ and $\bar{x_2^2}$ are computed for 8 different initial conditions of angles $\theta_1$ and $\theta_2$ at each $m_2$ using an averaging time of $T = 1000s$. time-averaged $\bar{x_2}$ converges to a value of zero due to the oscillating nature of the system, whereas the time-averaged of its square is non zero. 100 uniformly spaced values of $m_2$ between $[0.01, 6]$ are used and Fig. 6.5(b) and Fig. 6.6(b) show the values of $\bar{x_2}$ and $\bar{x_2^2}$ respectively, plotted versus $m_2$.

A standard linear central difference ODE solver is used to calculate the time-accurate solution of the sensitivity problem at $m_2 = 4$ with $dt = 10^{-3}s$. Sensitivities of $x_2$ and $x_2^2$ are plotted up to $T = 100$ in Fig. 6.7(a) and Fig. 6.8(a) where the values oscillate and grow to higher values of order $10^{30}$, these values continue to grow by several orders of magnitude for longer time periods for both $x_2$ and $x_2^2$. Using the stabilized solver developed by Bhatia and Makhija [14], the direct and adjoint sensitivities remain bounded to smaller values during the simulation presented respectively in Fig. 6.7(b) and Fig. 6.8(b) and Fig. 6.7(c) and Fig. 6.8(c) and show convergence for increasing averaging time for both quantities at hand.

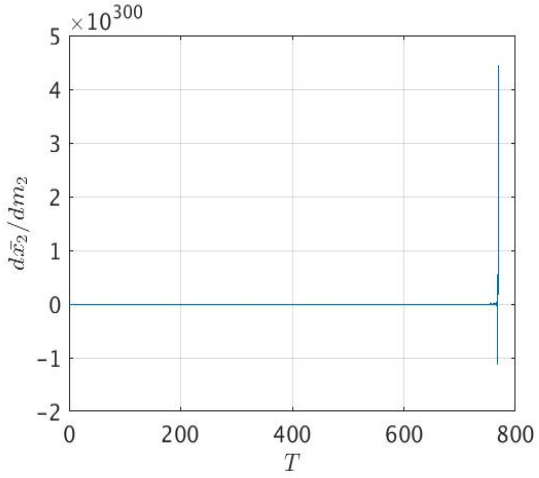


(a) Sensitivity with standard ODE solver

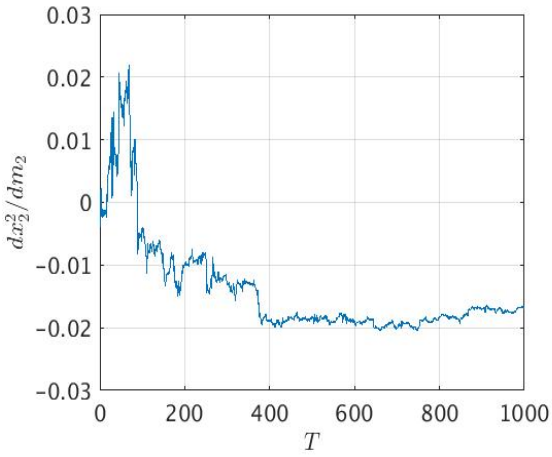


(b) Direct sensitivity

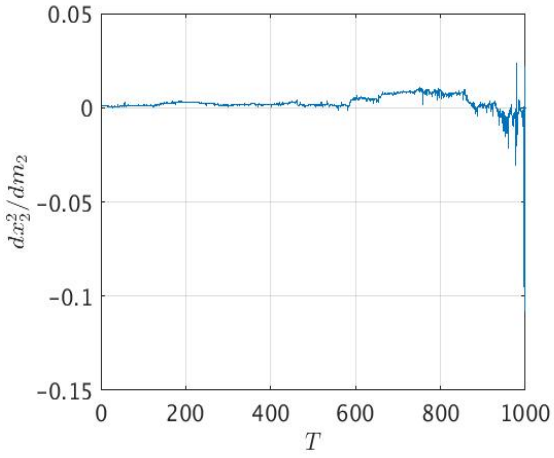


(c) Adjoint sensitivity

Figure 6.7: Sensitivity convergence of $d\bar{x}_2/dm_2$ at $m_2 = 4$.

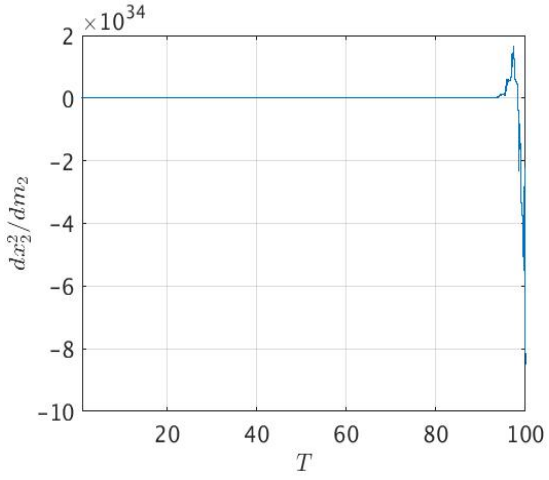


(a) Sensitivity with standard ODE solver

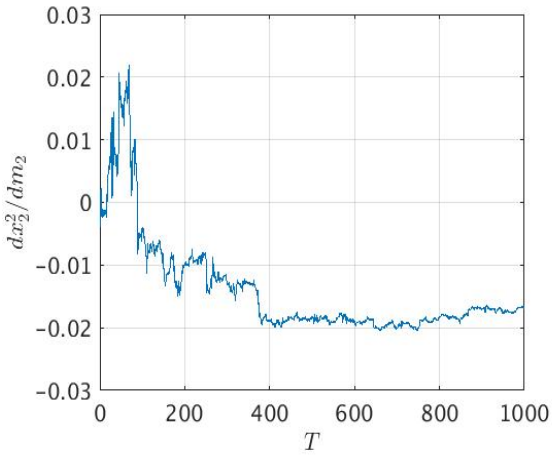


(b) Direct sensitivity

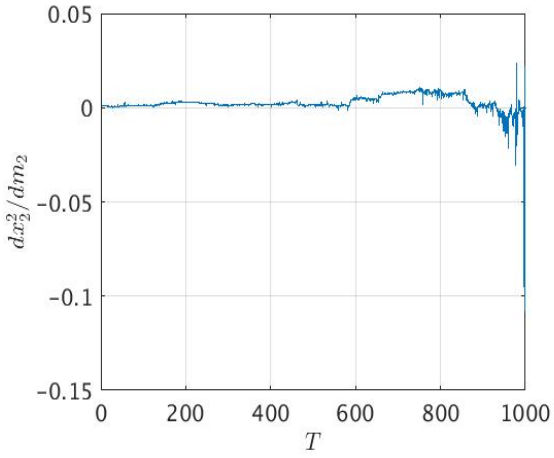


(c) Adjoint sensitivity

Figure 6.8: Sensitivity convergence of $d\bar{x_2^2}/dm_2$ at $m_2 = 4$.

The adjoint problem is solved backward in time, therefore the sensitivity values start from zero at the respective time and increase towards $t = 0$. This is an important distinction between the direct and adjoint approaches. Direct sensitivity solves the problem in forward

time and allows a control on termination of the time integration whereas the adjoint method solves the problem backward in time and requires integration from final time to $t = 0$ before the the time-averaged adjoint sensitivity can be used.

Different values of amplification factor have been used to study the influence of $\bar{a}$ on the convergence of sensitivities of time-averaged quantities. In Fig. 6.9 and Fig. 6.10 the values of $d\bar{x_2}/dm_2$ and $d\bar{x_2^2}/dm_2$ are computed for $100$ uniformly spaced values of $m_2 \in [0.01, 6]$ with 8 different initial conditions at each $m_2$. The initial values assume $\theta_1 = \theta_2 = \frac{\pi}{2}$ and $\dot{\theta_1} = \dot{\theta_2} = 0$. An averaging duration of $T = 1000s$ is used for all results with $dt = 0,001s$ and $1000,000$ time-steps for the nonlinear solver. Confidence intervals are plotted for both the direct and adjoint sensitivity values using the mean and standard deviation at each $m_2$.

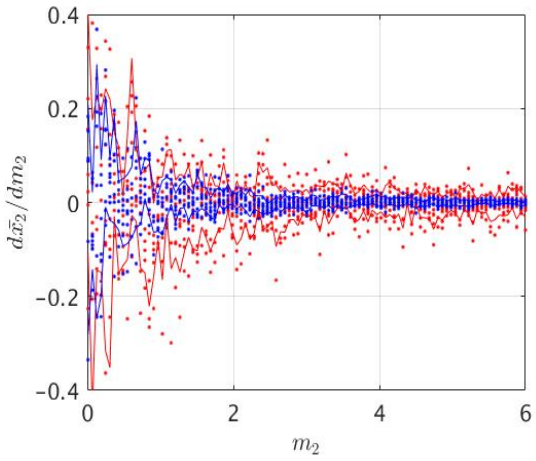


(a) $\bar{a} = 1$

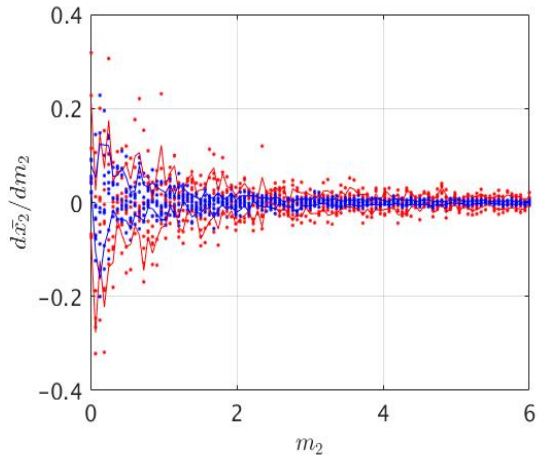


(b) $\bar{a} = 0.8$

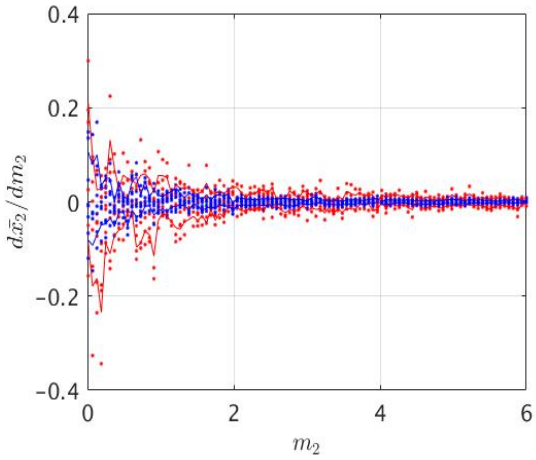


(c) $\bar{a} = 0.6$

Figure 6.9: Direct and adjoint sensitivities $d\bar{x}_2/dm_2$ for different amplification factors.

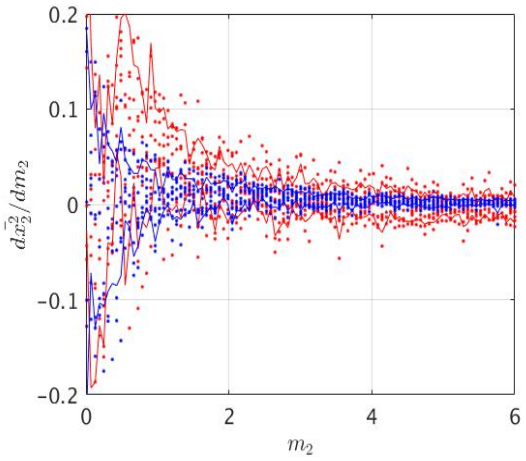


(a) $\bar{a} = 1$

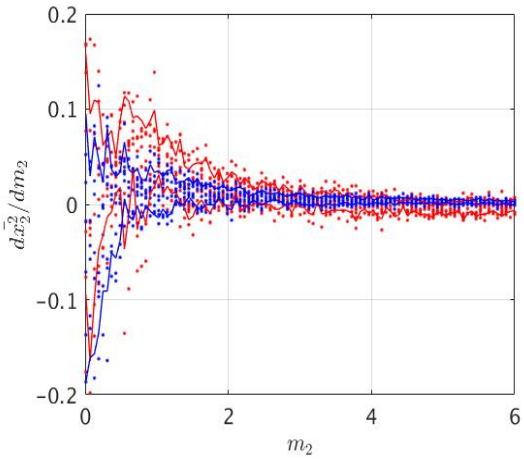


(b) $\bar{a} = 0.8$

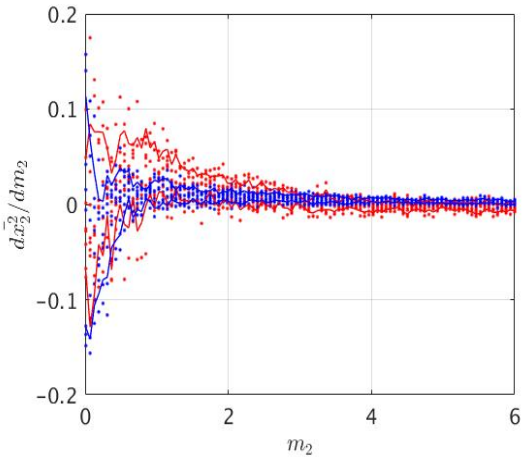


(c) $\bar{a} = 0.6$

Figure 6.10: Direct and adjoint sensitivities $d\bar{x}_2^2/dm_2$ for different amplification factors.

It can be observed from the two figures Fig. 6.9 and Fig. 6.10 that as the mass $m_2$ increases, both direct and adjoint sensitivity values decrease and reach a value of zero. However, as the amplification factor increases, the accuracy of the sensitivity results re-

duces and a larger spread in the range of smaller mass values is observed. Different results are obtained using the direct and adjoint sensitivity analyses for the same cases which is a result of the fact that the stabilization solver chooses time-step size independently for each sensitivity solution.

The influence of averaging time $T$ on the accuracy and convergence of quantities and their sensitivities is studied for $dt = 1.e-3s$. Three different values of amplification factor $\bar{a} = 0.6, 0.8, 1$ are studied. The results are shown in Fig. 6.11(a) and Fig. 6.11(b) for $\bar{x_2}$ and $\bar{x_2^2}$ respectively. As the Averaging time increases, $\bar{x_2}$ converges to zero and becomes less sensitive to initial values whereas for $\bar{x_2^2}$ different initial conditions result in different time-averaged quantities forming a band of nonzero values that gets narrower as $T$ increases

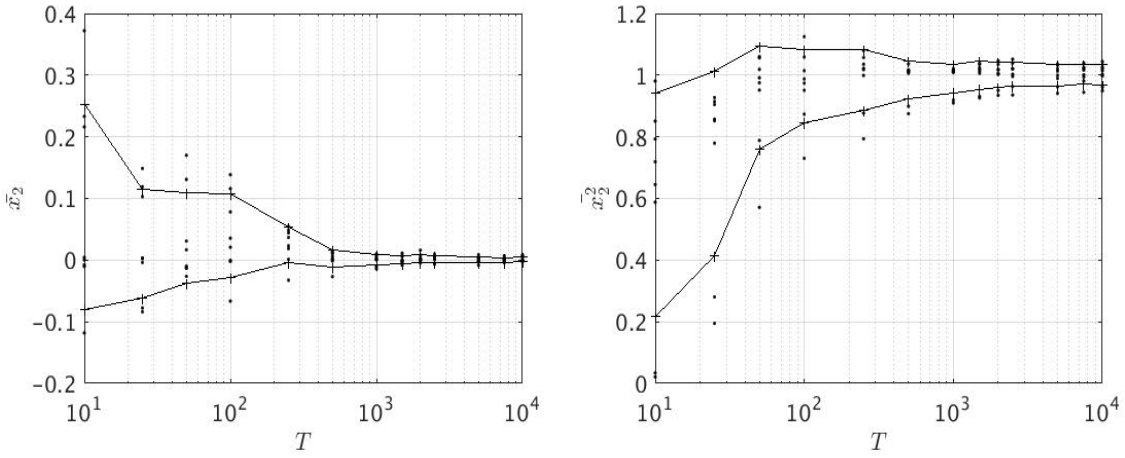


(a) Convergence of $\bar{x_2}$

(b) Convergence of $\bar{x_2^2}$

Figure 6.11: Convergence of time-averaged $\bar{x_2}$ and its square $\bar{x_2^2}$ at $m_2 = 4$ and $\bar{a} = 1$.

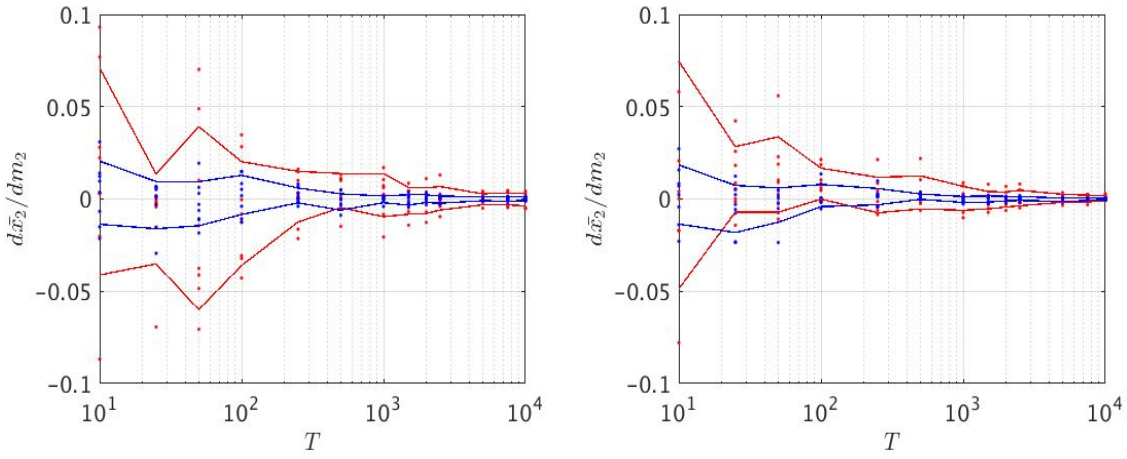


(a) $\bar{a} = 1$ (b) $\bar{a} = 0.8$

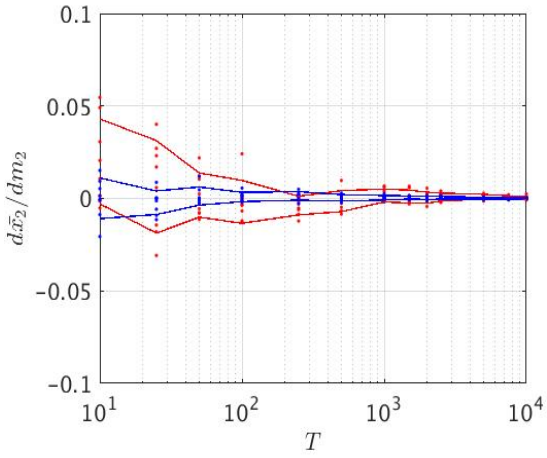


(c) $\bar{a} = 0.6$

Figure 6.12: Convergence of the sensitivities for different amplification factors at $m_2 = 4$.

Fig. 6.12 and Fig. 6.13 represent the convergence of the sensitivities $d\bar{x_2}/dm_2$ and $d\bar{x_2^2}/dm_2$ respectively for $\bar{a} = 0.6, 0.8, 1$. Both figures show that as the averaging time increases, the direct and adjoint method are producing sensitivity values, $d\bar{x_2}/dm_2$ and

$d\bar{x}_2^2/dm_2$, that are independent of the initial conditions. However, the final values are seen to depend on the choice of $\bar{a}$ for both time-averaged quantities. The smaller the amplification factor $\bar{a}$ is, the narrower the confidence intervals for both direct and adjoint sensitivity.

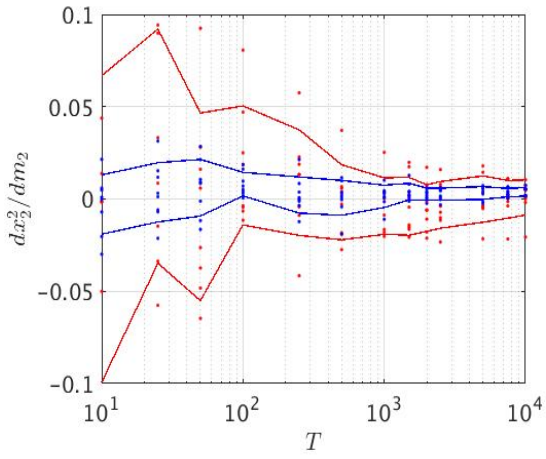


(a) $\bar{a} = 1$

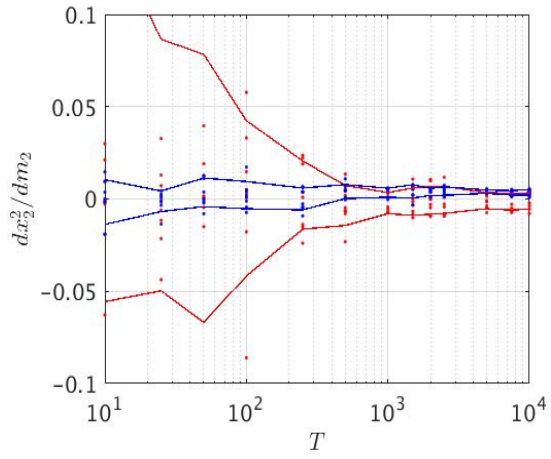


(b) $\bar{a} = 0.8$

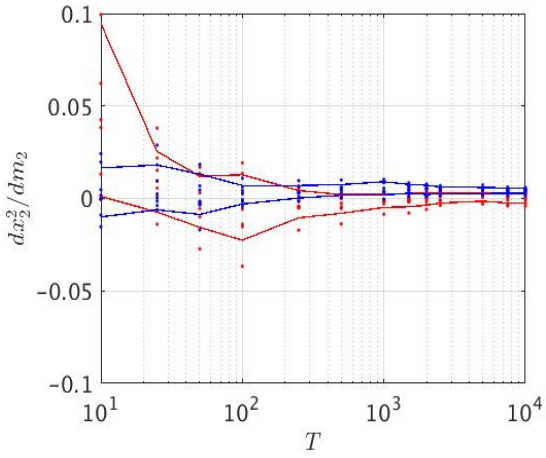


(c) $\bar{a} = 0.6$

Figure 6.13: Convergence of the sensitivities for different amplification factors at $m_2 = 4$.

From these figures, one can conclude that the sensitivities of the time-averaged $\bar{x_2}$ with respect to $m_2$ converges in less time steps than the adjoint and direct sensitivities of $\bar{x_2^2}$.

# CHAPTER VII

# CONCLUSION

In this thesis, sensitivity analysis of nonlinear chaotic systems is studied. First, the famous Lorenz system is considered. Its bifurcation study is presented to deeply understand the system's response as its parameters vary. Different bifurcations have been observed mainly Hopf bifurcation, Limit cycle oscillations, stranger attractor and preiod doubling bifurcations.

Computing the sensitivity analysis of this chaotic system using the standard sensitivity analysis methods was not able to provide useful results even when arbitrary precision arithmetics was adopted. Because not only the sensitivity values were growing exponentionally but also no matter how high the averaging time is, the sensitivity values don't seem to stay stationary as the time varies.

A new stablized solver approach for direct and adjoint sensitivity analysis of time-averaged quantities of chaotic systems is discussed. The new stabilized time-integrator with a norm-based adaptive time-step control is used for time-integration of the linearized sensitivity equations of two nonlinear systems, Lorenz system and double pendulum system. This new approach is able to accurately and efficiently comput the direct and adjoint sensitivities of both nonlinear systems.

A study is conducted to investigate the convergence of time-averaged quantities of chaotic systems and their sensitivities and to also get an understanding of how the definition of a quantity-of-interest might influence the number of iterations required to converge the sensitivity values. Results show that the approach computes accurate sensitivity values computationally order of magnitude lower than competing approaches and no extra cost is required to compute the sensitivity of squared time-averaged quantities.

Sensitivity analysis of other large-scale systems such as a chaotic beam response and flow over an airfoil is currently underway as long as a mathematical proof for the approach. Future workwork will consider, among other aspects, new strategies for adaptive time-step control and automatically choose the appropriate value for $\bar{a}$.

REFERENCES


[1] "Chaos:Meaning and History How a Word for a Void Came to Mean a Confused Mass", $www.merriam - webster.com$, 2019,(Online). Available: https://www.merriam-webster.com/words-at-play/chaos-meaning-and-history. (Accessed: 02- Jan- 2019).

[2] S. H. Kellert, "In the wake of chaos: Unpredictable order in dynamical systems", *The University of Chicago Press*, 1993.

[3] E. N. Lorenz, "Deterministic nonperiodic Flow", *Journal of The atmospheric Sciences*, 20, 1963, pp. 130-131.

[4] D. Ruelle, F. Takens, "On the nature of turbulence", *Comm Math Phys*, vol. 20, pp. 167-192, 1971.

[5] R. Dilao, T. Domingos, "Periodic and Quasi-Periodic Behavior in Resource Dependent Age Structured Population Models", *Bulletin of Mathematical Biology*, vol. 63, no.2, pp. 207-230, 2001.

[6] C. Kyrtsou, and W. Labys, "Evidence for chaotic dependence between US inflation and commodity prices", *Journal of Macroeconomics*, vol. 28, no. 1, pp. 256-266, 2006.

[7] S. Strogatz, "Nonlinear dynamics and chaos ;with applications to physics, biology, chemistry, and engineering", Cambridge, Mass., *Perseus Books Publishing*, 1994.

[8] A. Jameson, "Aerodynamic design via control theory", *Journal of Scientific Computing*, 3:233 260, 1988.

[9] D. Venditti, and D. Darmofal, "Grid adaptation for functional outputs: Application to two-dimensional inviscid flow", *Journal of Computational Physics*, 176:40-69, 2002.

[10] J.-N. Thepaut, and P. Courtier, "Four-dimensional variational data assimilation using the adjoint of a multilevel primitive-equation model", *Quarterly Journal of the Royal Meteorological Society* , 117(502):1225-1254, 1991.

[11] D. J. Lea, M. R. Allen, and T. W. Haine, "Sensitivity analysis of the climate of a chaotic system", *Tellus A: Dynamic Meteorology and Oceanography*, vol. 52, no. 5,2000, pp. 523-532.

[12] Q. Wang, R. Hu, and P. Blonigan, "Least Squares Shadowing sensitivity analysis of chaotic limit cycle oscillations", *Journal of Computational Physics*, vol. 267, 2014, pp. 210-224.

[13] A. Ni, and Q. Wang, "Sensitivity analysis on chaotic dynamical systems by non-Intrusive Least Squares Shadowing (NILSS)", *Journal of Computational Physics*, vol. 347, 2017, pp. 56-77.

[14] M. Bhatia, and D. Makhija, "Sensitivity Analysis of time-averaged Quantities of Chaotic Systems", *AIAA Journal*, pp. 1-12, 2019. Available: 10.2514/1.j057522.

[15] M. Bhatia, and L. Taoudi, "Assessment of Stabilized Sensitivity Analysis Approach For High-Dimensional Chaotic Systems", *AIAA SciTech Forum*, AIAA 2019-0170. Available:10.2514/6.2019-0170

[16] H. Oestreicher, "History of chaos theory", *Dialogues in Clinical Neuroscience*, vol.9, no. 3, 2007.

[17] P. S. Laplace, "Essai philosophique sur les probabilités", Truscott FW, Emory FL, trans, *A Philosophical Essay on Probabilities*, New York, NY: Dover, 1951.

[18] H. Poincaré, "Méthode nouvelles de la mécanique céleste", Goroff DL, transed, *New Methods of Celestial Mechanics in History of Modern Physics*, New York, NY: Springer-Verlag; 1992.

[19] E. N. Lorenz, "Predictability: does the flap of a butterfly's wings in Brazil set off a tornado in Texas?" Paper presented at: American Association for the Advancement of Science; 1972.

[20] J. M. Feigenbaum, "Quantitative universality for class of nonlinear transformations", *J Stat Physics*, pp: 25-52, 1978.

[21] R. M. May, "Simple mathematical models with very complicated dynamics", *Nature*, no. 261, pp 459-467, 1976.

[22] R. M. Murray, Z. Li, S. S. Sastry, "A Mathematical Introduction to Robotic Manipulation", *CRC Press*, 1994.

[23] J. Thuburn, *Climate sensitivities via a Fokker-Planck adjoint approach*, Q. J. R. Meteorol. Soc., 131 (2005), pp. 73-92.

[24] N. K. Yamaleev, B. Diskin, and E. J. Nielsen, "Local-in-time adjoint-based method for design optimization of unsteady flows", *Journal of Computational Physics* , vol. 229, no. 14, 2010, pp. 5394-5407.

[25] P. J. Blonigan, Q. Wang, E. J. Nielsen, and B. Diskin, "Least-Squares Shadowing Sensitivity Analysis of Chaotic Flow Around a Two-Dimensional Airfoil", *AIAA Journal*, vol. 56, no. 2, 2018, pp. 658-672.

[26] G. Eyink, T. Haine, and D. Lea, "Ruelles linear response formula, ensemble adjoint schemes and Lvy flights", *Nonlinearity*, vol. 17, no. 5, 2004, pp. 1867.

[27] P. J. Blonigan, and Q. Wang, "Multiple shooting shadowing for sensitivity analysis of chaotic dynamical systems", *Journal of Computational Physics*, vol. 354, 2018, pp. 447-475.

[28] D. Lasagna, "Sensitivity Analysis of Chaotic Systems using Unstable Periodic Orbits", *SIAM Journal on Applied Dynamical Systems*, vol. 17, no. 1, 2018, pp. 547-580.

[29] H. Haken, "Analogy between higher instabilities in fluids and lasers", *Physics Letters A*, vol. 53, no. 1, pp. 77-78, 1975.

[30] J. Yorke, and E. Yorke, "Metastable chaos: The transition to sustained chaotic behavior in the Lorenz model", *Journal of Statistical Physics*, vol. 21, no. 3, pp. 263-277, 1979.

[31] C. Sparrow, "The Lorenz Equations", New York: Springer-Verlag, 1982.

[32] W. Govaerts, "Numerical bifurcation analysis for ODEs", *Journal of Computational and Applied Mathematics*, vol. 125, no. 1-2, pp. 57-68, 2000.

[33] Dhooge, A., Govaerts, W., Kuznetsov, Y. A., MATCONT: a MATLAB package for numerical bifurcation analysis of ODEs, *ACM Transactions on Mathematical Software (TOMS)*, vol. 29, no. 2, 2003, pp. 141-164.

[34] Shibrot, T., Grebogi, C., Wisdom, J., Yorke, J. A., "Chaos in Double Pendulum", *American Journal of Physics*, vol. 60, no. 6, 1992, pp. 491-499.

[35] Gupta, M. k., Bansal, K., Singh, A. K. , Mass and Length Dependent Chaotic Behavior of a Double Pendulum, *IFAC Proceedings Volumes*, vol. 47, no. 1, 2004, pp. 491-499.

[36] L. Behera, I. Kar, "Intelligent Systems and Control Principles and Applications", *Oxford university Press*, 2009.

[37] "Arbitrary precision arithmetic", *En.wikipedia.org*,(Online). Available: $https : //en.wikipedia.org/wiki/Arbitrary_precision_arithmetic$. (Accessed: 10- Jan-2019).

[38] "About: GNU Multiple Precision Arithmetic Library", *Dbpedia.org* , (Online). Available:$http : //dbpedia.org/page/GNU_Multiple_Precision_Arithmetic_Library$. (Accessed: 10-Jan-2019).

[39] "The GNU MPFR Library", *Mpfr.org*. (Online). Available: https://www.mpfr.org/. (Accessed: 28- Jan- 2019).

[40] " Index listing for libs/multiprecision/doc/html/boostmultiprecision/1.61.0 " , *Boost.org*, (online). Available: $https://www.boost.org/doc/libs/1610/libs/multiprecision/doc/html/boost\_multiprecision/$. (Accessed: 10- Jan- 2019).

[41] "Chemistry: Chaos Theory Encyclopedia.com", *Encyclopedia.com*, (online). Available: https://www.encyclopedia.com/science/science-magazines/chemistry-chaos-theory. (Accessed: 08- Jan- 2019).